ULISSES ADONIS SILVA COSTA

NUMERICAL INVESTIGATION OF CONDENSING FLOWS IN A SUPERSONIC SEPARATOR

São Paulo
2020

ULISSES ADONIS SILVA COSTA

NUMERICAL INVESTIGATION OF CONDENSING FLOWS IN A SUPERSONIC SEPARATOR

Revised Version

Dissertation submitted to the Polytechnic School of University of São Paulo for Master in Science.

Concentration Area:
Energy and Fluid dynamics

Advisor:
Prof. Dr.Ernani Vittilo Volpe

São Paulo
2020

Este exemplar foi revisado e corrigido em relação à versão original, sob responsabilidade única do autor e com a anuência de seu orientador.

São Paulo, 08 de Setembro de 2020.

Assinatura do autor: 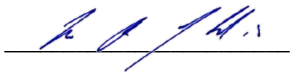

Assinatura do orientador: 

Catalogação-na-publicação

Costa, Ulisses Adonis Silva
Numerical Investigation of Condensing Flows in a Supersonic Separator / U. A. S. Costa -- versão corr. -- São Paulo, 2020.
71 p.

Dissertação (Mestrado) - Escola Politécnica da Universidade de São Paulo. Departamento de Engenharia Mecânica.

1.Nucleação 2.Separador supersônico 3.Gases não-ideais 4.Gás natural I.Universidade de São Paulo. Escola Politécnica. Departamento de Engenharia Mecânica II.t.

AGRADECIMENTOS

Primeiramente, eu gostaria de agradecer a Deus, sempre presente em minha vida, colocando no meu caminho pessoas especiais. Sei que em diversos momentos, quando eu não tinha mais forças, você me carregou em seus braços. Teus planos para minha vida foram muito maiores do que eu poderia imaginar.

A minha mãe , Léa , verdadeiramente a maior mestra e amiga da minha vida, que sempre acreditou em mim e apesar das circustâncias muitas vezes mostrarem o contrário, manteve a fé. Todas as minhas conquistas são dedicadas a esta incrível mulher, que muitas vezes abdicou da sua própria felicidade, para me ver feliz. A minha irmã Pamela, que sempre me incentivou e estendeu a mão quando mais precisei.

Dedico este trabalho a minha filha Vitória, meu pequeno grande milagre e agora a razão do meu viver. Minha filha amada, que um dia você possa entender o quanto a ciência e a educação são importantes para a vida.

Ao meu orientador Ernani Vittilo Volpe, pela compreensão, sábios conselhos e direcionamentos. Apesar de ser um dos homens mais brilhantes que conheci, minha verdadeira admiração por este homem está na enorme bondade que reside em seu coração. Verdadeiramente, um dos melhores seres humanos que conheci em toda minha vida. Agradeço também ao professor (e amigo) Arlindo e ao amigo Jairson, pelas risadas e conversas.

Ao meu grande amigo, irmão de universidade e colega de pesquisa Alexandre Martuscelli Faria. Agradeço pelas risadas, pelo ombro amigo, pelas palavras de correção e principalmente por nunca me abandonar. Meus mais sinceros obrigados. Ao amigo Lucas Kavabata por toda ajuda e dedicação dada a nossa pesquisa.

A Danielle Goto por todo companheirismo, ajuda, palavras de carinho, paciência conselhos e dedicação. Com certeza, boa parte dessa dissertação foi graças a você e a sua familia. Obrigado pelos jantares, almoços e por diversas vezes, um teto para eu dormir.

Aos meu primos e tios que nunca me abandonaram desde a morte de meu querido pai. Deixo expresso meu agradecimento especial ao meu primo Alessandro Silva que , definitivamente, é um dos maiores incentivadores da minha vida acadêmica.

Agradeço a Coordenação de Aperfeiçoamento de Pessoal de Nivel Superior pela bolsa que permitiu dois anos de formação acadêmica diferenciada e de qualidade. Agradeço a incrível oportunidade de pesquisa oferecida pelo Centro de Pesquisa para Inovação em Gás (RCGI) e pela bolsa complementar que me permitiu terminar este trabalho.

Aos meus amigos Kenji Okabayashi, Lucas Hodalck e Waldemar Gomes por estarem sempre presente em minha vida. A minha amiga Barbara Andrade, mesmo longe, sempre disposta a me escutar e dar bons conselhos. w

E por último , ao meu querido pai Raimundo. Sei que sempre esteve ao meu lado e nunca me abandonou. Cumpro a promessa feita em seu caixão. Um filho nunca se esquece.

"Epigraph"

Out of the night that covers me, Black
as the pit from pole to pole,
I thank whatever gods may be
For my unconquerable soul.

In the fell clutch of circumstance
I have not winced nor cried aloud.
Under the bludgeonings of chance
My head is bloody, but unbowed.

Beyond this place of wrath and tears
Looms but the horror of the shade,
And yet the menace of the years
Finds and shall find me unafraid.

It matters not how strait the gate,
How charged with punishments the
scroll
I am the master of my fate:
I am the captain of my soul.

- William Ernest Henley

RESUMO

As recentes descobertas de grandes volumes de hidrocarbonetos na costa, nos chamados reservatórios do pré-sal, reforçam o importante papel que o Brasil desempenhará no cenário energético mundial. Um dos grandes problemas presentes nessas áreas é a alta concentração de dióxido de carbono CO_2 associado ao gás natural, em reservas com um alto potencial de produção. A experiência operacional diz que também é necessário reduzir e controlar a presença de água, na forma líquida ou de vapor, presente no gás natural, para garantir seu processamento e transmissão com segurança. O separador supersônico, uma tecnologia inovadora baseada no resfriamento adiabático de um fluxo de gás submetido a um turbilhão, surge como uma nova e promissora técnica para remover dióxido de carbono e componentes gasosos de um gás natural. No entanto, o processo de condensação em um fluxo compressível em turbilhão ainda é pouco conhecido. Isso coloca sérios desafios ao design desses dispositivos. Como contribuição para superar esses desafios, este trabalho tem como objetivo investigar a nucleação de moléculas simples comparando diversas equações da taxa de nucleação associadas ao Método dos Momentos de Hill. A não idealidade dos gases é bem discutida e os fenômenos de mudança de fase para aplicação em um separador supersônico de gás natural são estudados considerando inicialmente a condensação da água. O modelo Euler acoplado ao método dos momentos foi utilizado para investigar os fluxos de condensação em não-equilíbrio nos bocais. Os resultados númericos foram verificados com dados experimentais disponíveis na literatura e houve uma melhora significativa na captura da onda de condensação.

Palavras-chaves: Separador supersônico, Nucleação, Condensação, Escoamento Bifásico, Gases

ABSTRACT

Recent discoveries of large volumes of hydrocarbons on the coast, in the so-called pre-salt reservoirs, reinforce Brazil's role as an important player in the world energy scenario. One of the most relevant issues presents in this areas is the high concentration of carbon dioxide CO_2 associated with natural gas in reserves with high production potential. The operating experience says that it is also necessary to reduce and control the presence of water, in liquid or vapor form, present in natural gas, to ensure its processing and transmission safely. The supersonic separation, an innovative technology based on the adiabatic cooling of a swirling gas flow, arise as promising new technique to remove carbon dioxide and gaseous components out of a natural gas. However, the process of condensation in a swirling compressible flow, is still poorly understood. This poses serious challenges to the design of those devices. As a contribution to overcoming those challenges, this work aims to investigate the nucleation of simple molecules the nucleation of simple molecules by comparing several nucleation rate equations associated with Hill's Method of Moments. The non-ideality of gases is well discussed and the phase change phenomena for application in a supersonic separator of natural gas are studied considering the condensation of water initially. The Euler model coupled to the method of moments was used to investigate non-equilibrium condensing flows in nozzles. The numerical results were verified with experimental data available in the literature and there was a significant improvement in the capture of the condensation wave.

Keywords – Condensation, Supersonic Separator, Two phase flow, Non-ideal gas, Nucleation.

LIST OF FIGURES

LIST OF TABLES

LIST OF SYMBOLS

u	gas velocity.
u'	velocity fluctuation
v	gas tangential velocity at the throat of nozzle
ρ_l	Density of liquid
ρ_v	Vapor density
σ	Droplet surface tension
m	Condensation mass per unit vapor volume per unit time
Z	compressibility factor
N_d	Droplet number density.
p:	Pressure.
r^*	Droplet critical radius.
r_d	Droplet radius.
R_v	Gas constant.
T_s	Saturation temperature at local pressure.
E	Total energy
h	Vapor total enthalpy
h_{lg}	Latent heat of condensation
S	Supersaturation of the vapor
S_m	Vapor continuity equation source term
S_u	Vapor momentum equation source term
S_h	Vapor energy equation source term
S_y	Liquid continuity equation source term
k_B	Boltzmann constant
k_{eff}	Effective thermal conductivity
J_{CNT}	nucleation rate calculated by classic nucleation theory.
J_{ICCT}	nucleation rate calculated by Internally Consistent Classical Theory.
J_f	nucleation rate calculated by correction factor f.
q_c	condensation coefficient

CONTENTS

1 INTRODUCTION

According to 2018 edition of the IEA 'Global Energy and CO_2 Status Report', the energy demand worldwide grew by 2.3%, the fastest pace in a decade, driven by solid growth of the global economy and higher heating and cooling needs in some parts of the world. Governments continue their efforts to face the dual challenge of producing a sufficient amount of energy with high quality, associated with environmental sustainability. In this scenario, natural gas will play a very important role in the composition of the new global energy matrix, based on a future low carbon economy.

Recent discoveries of large volumes of natural gas on the coast, in the so-called pre-salt reservoirs, reinforce Brazil's role as an important player in the world energy scenario. Information collected from the first drilled wells indicates reservoirs with carbon dioxide levels above the national average, although concentrations vary over the large pre-salt area, as seen in Fig.1:

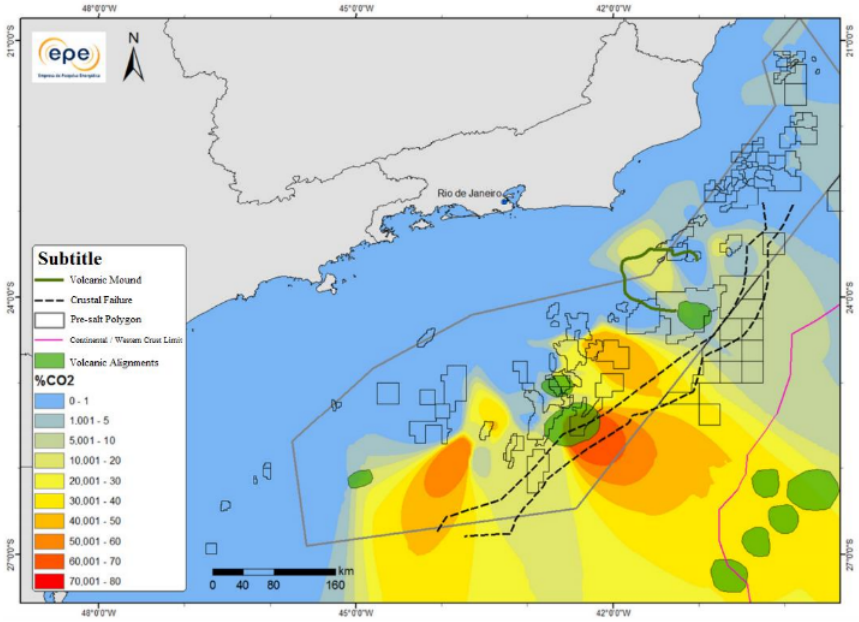

Figure 1: CO_2 concentration map in brazilian pre-salt.
Source: [EPE, 2012]

One of the pertinent challenges related to the development of these reservoirs is to remove the excess of CO_2 from the natural gas mixture, in order to make it economically attractive, through modern separation processes. Petrobras has invested in separation systems in FPSOs - Floating Production Storage and Offloading - in order to facilitate the re-injection of carbon dioxide in offshore caves (carbon capture and storage technique), thus reducing the emission of harmful gases to the environment. Today, the most common purification processes are:

- Adsorption processes: Use adsorbers to promote separation at molecular level. As an advantage it has high efficiency for separation with low CO_2 content, at low pressures. However, it is not very efficient for high concentrations (efficient for 0.5 to 3% in molar fraction), since the maintenance cost of the adsorber material is high.
- Amine units: Also known as the absorption process, it uses a solvent for CO_2, monoethanolamine - MEA. There is a need for solvent re-circulation and reheating expenses in order to regenerate the solvent, which makes the costs proportional to the amount of gas separated, being a process usually limited to concentrations of 3 to 25% in molar fraction.
- Membrane process: In essence, gas separation membranes are thin films that selectively transport gases through the membrane based on differences in permeabilities of the species flowing through the membrane. It is very useful for a wide variety of molar concentrations, however it is complex and very expensive for multi-component mixtures.

It is clear that most current separation processes, such as membrane processes, amine units, and adsorption do not fit the characteristics of the pre-salt natural gas. In addition, these technologies have a size proportional to the amount of impurities removed, thus having to occupy a good portion of the expensive space available in FPSOs.

The supersonic separator emerges as an innovative and revolutionary solution to solve the challenges of gas processing.This technology is based on the adiabatic cooling of swirling gas flow in a supersonic nozzle, which separates condensed phase from the mixture using centrifugal forces.This device could be easily adopted in the natural gas transmission pipelines, in order to condense and separate the hydrocarbons from dioxide carbon.

1.1 The Supersonic Separator

The supersonic separator's technology was first developed at approximately 50 years ago and has since been optimized. The leading manufacturers of this technology are Engo 3S and Twister BV. The first is a Russian group and the second is a joint venture between Shell and Beacon Group, both of which were recently founded - mid-2000 - and with products of different geometries but with the same purpose as shown in Figures 2 and 3. The primary difference between the models is in the way of generating swirl .

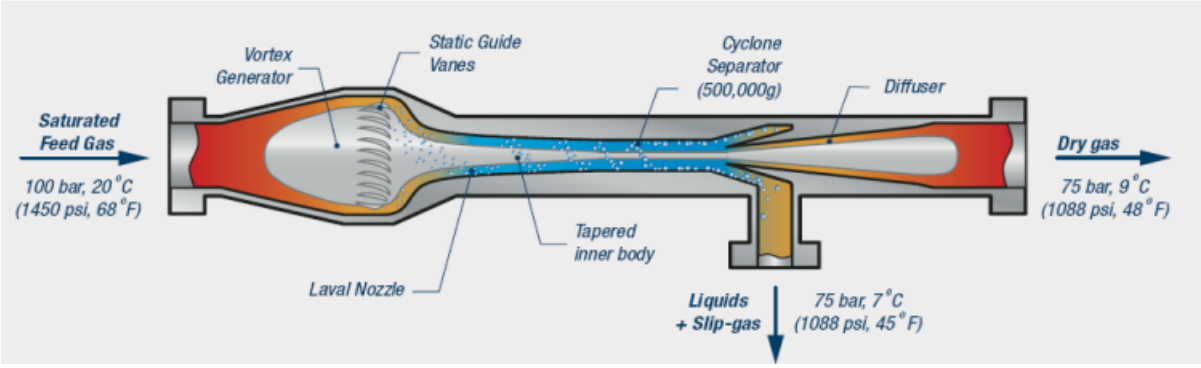

Figure 2: Cross-section of Twister Tube.
Source: [TWISTER, 2016]

The Engo 3S model uses conventional stationary blades, whereas the Twister BV model has a central body where the blades are fixed, which impels rotation to the flow. In addition the contraction or expansion occur due to the increase or decrease of the cross-section of the central body along the length of the flow. It is different from the first model, which had a conventional Laval nozzle.

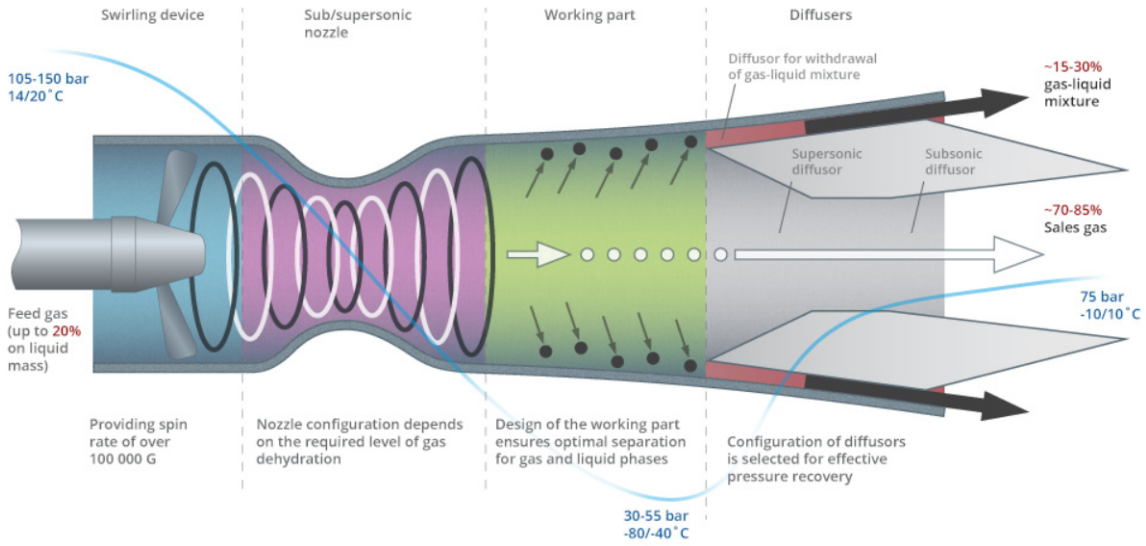

Figure 3: Cross-section of ENGO 3S Tube.
Source: [ENGO-ENGINEERING, 2017]

Although the above description does not contain much technical details, they should not be construed as limiting the development of this work but merely illustrations of some of the presently preferred device by the oil and gas market.

1.2 Natural Gas

The natural gas processed at the wells will have different range of composition depending on type, depth, and location of the underground reservoirs of porous sedimentary deposit and the geology of the area. Natural Gas (NG) is a hydrocarbon gas mixture, consisting primarily of methane, derived from the decomposition of fossilized organic matter over millions of years. Other components found in natural gas include carbon dioxide, helium, hydrogen sulfide, and nitrogen. Because of the different sources, the composition of natural gas is never constant and can vary significantly. The Table 1 shows an average composition of natural gas:

Table 1: Natural Gas average composition.
Source: [MONTEIRO J./ SILVA, 2010]

Substance	*Volume* (%)
Methane	88,60
Propane	2.7
Butane, Pentane, Hexane	7.3
Carbon Dioxide	0.5
Nytrogen	0.9

According to the ANP [AGÊNCIA NACIONAL DE PETRÓLEO, 2019] the natural gas production has maintained growth for the ninth consecutive year, with an increase of 1.8%, thus totaling 40.9 billion m^3 in 2018. In the decade 2009-2018, national natural gas production showed an average growth of 6.6% per year and accumulated 93.3%. Technological innovations have increased the efficiency and cost-competitiveness it has allowed natural gas extraction from deep waters formation which were previously considered not profitable.

1.3 Problem description

Brazilian pre-salt has a great potential for natural gas production, however, there are technological challenges to make commercial use viable. The high level of contamination by CO_2 and other impurities such as water vapors implies high costs for separation and utilization of natural gas.

Today, the separation of these contaminants is done through membrane separation plants installed in floating Production Storage and Offloading (FPSOs). These equipment are costly, waste a lot of energy and occupy an important area of the production unit.Therefore, the natural gas production potential depends on the development of new technologies for the separation of its impurities.

1.4 Project Goal and Motivation

In the course of world economic development, the basic question is how sustainable development and a robust energy matrix can co-exist in order to secure resources for future generations. The Research Center for Gas Innovation (RCGI), based at the University of São Paulo (USP), has been tasked by the Shell Oil Company and FAPESP to develop a prototype of supersonic separator that can be tested in a few years. This prototype

shall provide the sets of experimental data for validation purposes, which are required to advance the technologies for separation of natural gas.

Two-phase condensing flows are very common in many industrial applications and depending on how and where it takes place, it can lead to a degradation of a component's performance or, in this particular case, a efficacy decrease in the gas separation process. Thus, the physical understanding and accurate numerical modeling of the condensation process should be of great relevance to the design process.

The present work focuses on understanding the condensation phenomena in the supersonic separator. Primarily, this will consist of selecting an appropriate equation of state model that best represents the behavior of gases in the flow,and, an appropriate condensation rate equation that can faithfully represent the location of the condensation wave. A significant part of the work will be to assist in the development and implementation of numerical tools to model the condensation phenomena in the open source SU2 (Stanford University Unstructured) . The SU2 solver is an open-source unstructured edge flow-solver, written in C++, under development at various universities, including Stanford University, TUDelft and the CFD community .

Therefore, the principal aim of the present study is to gain physical insight into the modeling of nucleation and growth theories that involve all condensation process.

1.5 A brief review of first studies

The first investigation in the field of condensation was done by John Aitken [AITKEN, 1874], who conducted experiments on atmospheric dust to study to the formation of clouds and mists. However, only in 1887 a more detailed investigation on this assumption was made by C.T. Wilson, who developed a refined expansion cloud chamber which the initially used to study homogeneous nucleation. This work analyzed the behavior of water vapor mixed with air and other gases when subjected to rapid expansions.

Some years later, Stodola [STODOLA, 1927] published his own results for nozzle expansions and created an experimental technique of light scattering to detect the occurrence of condensation. In 1937, Yellot [J.I.YELLOT; HOLLAND, 1874] detected a point, where an abrupt change occurs in the static pressure in a nozzle with condensation. Subsequently explained by Kennan [KEENAN, 1941] in Fig. 4, the stream enters the nozzle (1) as dry super-heated vapor and during its passage through the nozzle, it expands to the sonic condition at the throat.

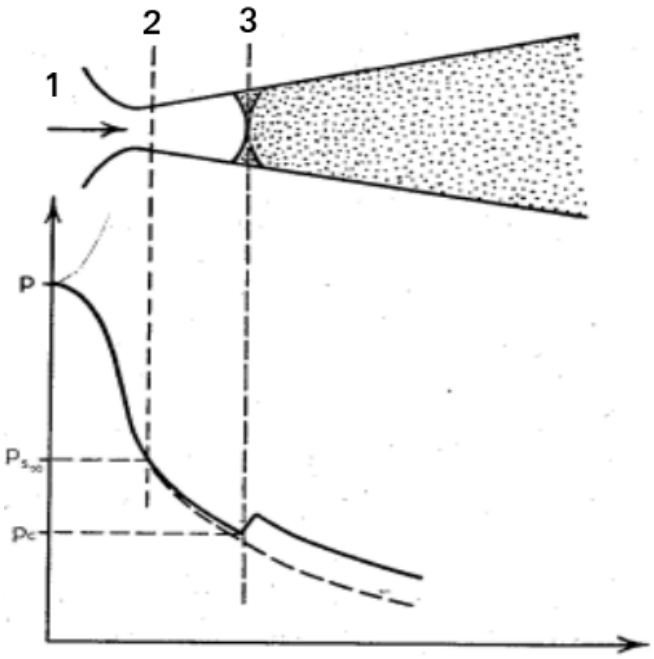

Figure 4: Comparison of static pressure behavior in a nozzle with and without condensation.

Source: [STEVER, 1958]

The vapor pressure decreases according the laws of isentropic expansion until it reaches at point (saturation vapor pressure), represented by a solid line . Between the points (2) and (3) in Fig. 4, small droplets begin to form and grow in the vapor. The associated nucleation rates of early drops are so low that steam continues to expand as single-phase dry vapor in a meta-stable, super-cooled or supersaturated state. Depending on the local conditions and the rate of expansion, the nucleation rate increases dramatically and its maximum at point (3). This area is termed nucleation zone and an abrupt pressure rise occurs.

The first investigation of the condensation of water vapor in supersonic wind tunnels, was made by Herman and Wieselsberger in 1934. In 1942, an experimental investigation was conducted by Wagner. C, investigating the expansion of dry air at room temperature and atmospheric pressure in a hypersonic wind tunnel, he realized that resulted in a supersaturate state for nitrogen and oxygen . Laboratory studies of nucleation and droplet growth have principally been carried out in converging-diverging nozzles and many such investigations have been reported.

Young and White [YOUNG, 1992] were the first to perform 2D simulations for a condensing steam flow. Jan Halama [HALAMA, 2012] performed 2D simulations in the supersonic Barschdroff nozzle for an inviscid case using complete Eulerian approach.

Gyarmathy [GYARMATHY, 2015] conducted research on the droplet growth process and set up the mathematical model of the drop-let growth stage in consideration of the effect of incondensable gas.

Azzini and Pinni [AZZINI, 2017] investigated High-pressure non-equilibrium condensing flows through a 2D Euler model coupled to the method of moments for the physical characterization of the dispersed phase.

2 THERMODYNAMIC ASPECT

The major objective of this chapter is introduce the importance of establish certain thermodynamic relationships useful in the investigation of the non-ideal behavior of the gases. The non-ideal state of the fluid provides a set of properties that impact not only the equations governing compressible flow but also provide insight for a suitable design.

A brief summary of historical development of empirical equation of state will be presented to the reader. An extensive analysis was performed to find the appropriate equation to the challenge of correctly modeling the thermodynamic behavior of the system.

2.1 Thermodynamic Relationship

For practical applications of thermodynamic laws, system properties must be available. The fundamental thermodynamic variables involved in these processes are: temperature (T), pressure (P), internal energy (U) and entropy (S). The first and second law of thermodynamics can be combined into what is known as the fundamental thermodynamic relationship, which describes all changes in thermodynamic state functions.For a quasistatic reversible change, we can express it as a function of internal energy as:

$$dU = TdS - PdV \tag{2.1}$$

This is just an expression of the fundamental thermodynamic relationship. Using different variables, we can express it in terms of Helmholtz's free energy (F) as:

$$dF = -PdV - SdT \tag{2.2}$$

in terms of the enthalpy (H) as:

$$dH = VdP + TdS \tag{2.3}$$

and rewritten in terms of Gibbs free energy (G) as:

$$dG = VdP - SdT \tag{2.4}$$

2.2 Gibbs Energy Formulation

The Gibbs free energy is an important means for predicting chemical reactions. The Fundamental Equation for a single component was express in Eq 2.4. Using the first order partial derivatives, we can obtain the three equations necessary to define the state of a system:

$$-S = g_1(T, P, N) = G_T \tag{2.5}$$

$$V = g_2(T, P, N) = G_P \tag{2.6}$$

$$U = g_3(T, P, N) = G_N \tag{2.7}$$

With some mathematical manipulations and simplifications, we can find the following equations in first order in mass:

$$-\left(\frac{\partial S}{\partial T}\right)_P = -\frac{1}{N}\left(\frac{\partial S}{\partial T}\right)_{P,N} = g_{11}(T, P) \tag{2.8}$$

$$-\left(\frac{\partial V}{\partial P}\right)_T = -\frac{1}{N}\left(\frac{\partial V}{\partial P}\right)_{T,N} = g_{22}(T, P) \tag{2.9}$$

$$\left(\frac{\partial V}{\partial T}\right)_P = -\left(\frac{\partial S}{\partial P}\right)_T = -\frac{1}{N}\left(\frac{\partial V}{\partial T}\right)_{P,N} = g_{12}(T, P) \tag{2.10}$$

on the left side, we can omit the subscript N (mole numbers) when expressing partial derivatives of intensive variables for single component systems. These derivatives are related to three widely proprieties: the isothermal compressibility (κ_T), heat capacity at constant pressure(C_p) and the coefficient of thermal expansion (α_p).

$$C_p = -T\left(\frac{\partial S}{\partial T}\right)_P \tag{2.11}$$

$$\kappa_T = -\frac{1}{V}\left(\frac{\partial V}{\partial P}\right)_T \tag{2.12}$$

$$\alpha_p = -\left(\frac{\partial S}{\partial P}\right)_T = -\frac{1}{V}\left(\frac{\partial V}{\partial T}\right)_P \tag{2.13}$$

The Gibbs-Duhem equation for a pure substance is given by:

$$d\mu = -SdT + VdP \tag{2.14}$$

replacing S and V as functions of T and P, using the equations(2.5 -2.7) and integrating in two steps from a reference state, where u is set equal to an arbitrary value of u^0, will result in the following expression:

$$\mu = \mu^0 + \int_T^{T^0} [g_1(T,P)]_{p^0}\, dT + \int_P^{P^0} [g_2(T,P)]_T\, dP \tag{2.15}$$

we know that S and V are state properties, so:

$$dS = \left(\frac{\partial S}{\partial T}\right)_P dT + \left(\frac{\partial S}{\partial P}\right)_T dP \tag{2.16}$$

$$dV = \left(\frac{\partial V}{\partial T}\right)_P dT + \left(\frac{\partial V}{\partial P}\right)_T dP \tag{2.17}$$

substituting the second-order partial equations (Eq.2.11 - Eq.2.13):

$$dS = \frac{C_p}{T} dT + \alpha_P \, V dP \tag{2.18}$$

$$dV = \alpha_P \, V dT - \kappa_T \, V dP \tag{2.19}$$

integrating from a reference state T^0 and P^0, we have

$$S = S^0 + \int_T^{T^0} \left(\frac{C_p}{T} \right)_{P^0} dT - \int_P^{P^0} (\alpha_p V)_T \, dP \tag{2.20}$$

$$V = V^0 + \int_T^{T^0} (\alpha_p V)_{p^0} \, dT - \int_P^{P^0} (\kappa_T \, V)_T \, dP \tag{2.21}$$

rearranging the above equations and substituting in Eq. 2.15:

$$\Delta G = \Delta \mu = -(T - T^0) S^0 + (P - P^0) V^0 - g'(T, P, T^0, P^0) + g"(T, P, T^0, P^0) \tag{2.22}$$

for a isothermal process, we can note that ΔG is no longer dependent of S^0 and Eq. 2.22 can be expressed by:

$$\Delta G|_T = \int_{P_1}^{P_2} V dP \tag{2.23}$$

physically, this equation represents the negative of reversible flow work for an isothermal process.

2.3 Termal Equation of State

Equations of state play a very important role when an engineer wants to develop and analyze new industrial processes. A few hundred evaluations of thermodynamic properties are required under different operating conditions so that computationally inexpensive models can be used for this purpose. The starting point for any study involving gas thermodynamics is generally the use of the simplest form known as the ideal gas law.

$$PV = nRT \tag{2.24}$$

where P represents the gas pressure, V denotes some closed volume, n represents the number of moles inside a volume V, R is the specific gas constant and T represents the temperature of the gas. As an initial approach, we assume that gas molecules are so small that their actual volume can be considered negligible compared to the total gas volume and their respective attractive forces are weak enough to become negligible.

While ideal gases are strictly a theoretical conception, non-ideal gases can behave ideally under certain conditions. Thermodynamic systems at high temperatures and low pressures allow non-ideal gases to be estimated as ideal gases. The ideal gas law works well for small molecules, low pressures and high temperatures.

In this work, the Ideal Gas Law served mainly as an initial step to obtain information about the system. While accuracy is not the primary consideration in numerical simulations using the Ideal Gas Law, it offers ease of calculation and provides physical insights into the system.

2.4 Non-Ideal Gas

Many equations of state have been proposed to represent thermodynamic processes with greater precision than ideal gas law for regions where it does not apply. The operating conditions of the supersonic separator are characterized by compressible flow, moderate temperatures and super-critical pressures, and because of this, non-ideality effects are a prominent feature and must be taken into account within the numerical structure to accurately model fluid behavior.

Unfortunately, state reference equations are not available for most fluids. In general terms, the availability of precise multiparameter equations of state is inversely proportional to the molecular complexity that characterizes the fluid.(citing the P.Colona and A. Guardone comment[1]). A useful parameter for measure how much the thermodynamic properties of a real gas deviate from those expected of an ideal gas is the compressibility factor (Z). Also called “deviation factor”, can be explained as the ratio between the actual volume of a real gas and the predicted volume of the ideal gas at the same temperature and pressure as the actual volume. The definition of the compressibility factor is expressed

as:

$$Z = \frac{V_{actual}}{V_{ideal}} \tag{2.25}$$

introducing the compression factor in the gas law :

$$PV = ZnRT \tag{2.26}$$

for an ideal gas, Z = 1, but when the compressibility factor deviates from this value, the gas may be considered to be increasingly non-ideal.

2.5 Speed of sound Non-Ideal Gas

The fundamental equation for the speed of sound in a gas can be expressed as:

$$c^2 = \frac{\partial P}{\partial \rho} \tag{2.27}$$

Pressure disturbances in the fluid are observed to cause small changes in temperature due to the compression and expansion effect of the passing disturbance. This process has (approximately) isentropic behavior, therefore gas particles undergo near reversible and adiabatic compression and expansion [NEDERSTIGT, 2010]. The propagation velocity of a pressure disturbance in a medium can be express as:

$$c^2 = -v^2 \left(\frac{\partial P}{\partial \rho}\right)_s \tag{2.28}$$

The partial derivative $(\partial P/\partial \rho)_s$ is simply the derivative of the pressure-volume isentrope. The speed of sound in a non-ideal gases can be express as:

$$c^2 = \gamma_{PV} ZRT \tag{2.29}$$

and the Mach number for a non-ideal gases is:

$$M = \frac{u}{\gamma_{PV} Z R T} \tag{2.30}$$

2.6 Van der Waals Equation

The first step in understanding the non-ideality of gases was taken in 1873, by Johannes Diderik van der Waals, in his doctoral thesis ("On the Continuity of the Gaseous and Liquid State"), introducing the equation of state which has made the first connection between microscopic interaction of molecules and the macroscopic behavior of substances.The Van der Waals equation such as its derivatives is summarized in Table 2.

Table 2: Summary of Van der Walls equations of state.

$$P = \frac{RT}{(v-b)} - \frac{a}{v^2} \tag{2.31}$$

$$e(T,v) = c_v T - \frac{a}{v} \tag{2.32}$$

$$s(T,v) = c_v ln T + R ln(v-b) \tag{2.33}$$

$$a = \frac{27}{64}\frac{R^2T^2}{P_c} \qquad b = \frac{27}{64}\frac{R^2T^2}{P_c} \tag{2.34}$$

where constant a represents a correction for the inter-molecular forces and constant b adjusts the volume occupied by the gas particles. Both have positive values and are characteristic of the individual gas.

It is well known that the van der Waals equation is a cubic equation in v and this means that: at a given temperature, each pressure value corresponds to three specific volume values. To better understand what this means, we can state that the first values of the two roots found (representing specific volumes v_1 and v_2) correspond to the physically existing states of liquid and vapor. However, the third root (v_3) corresponds an unstable

and physically non-existent state. In order to illustrate the above explanation, we can observe the isotherm in Figure 5.

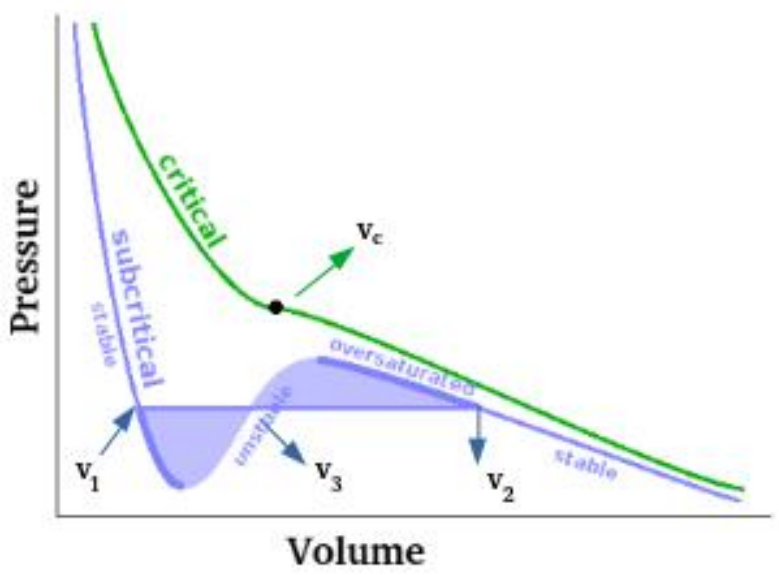

Figure 5: Van der Waals isotherms
Source: [ABERYSTWYTH..., 2018] - Modified by the Author.

The root v_1 is the smallest of the three and represents the liquid state; by other hand , the largest value ,represented by v_2, is the vapor root . A non-physical root (v_3) exists between the other two. We can note that the possibility of three real roots is restricted to the case of sub-critical conditions ($T < T_c$).

At high temperatures, the cubic equation predicts three real and equal roots at a special and particular point know as critical point. In $v = v_c$, vapor and liquid properties are the same and the following conditions are valid:

$$\left(\frac{\partial p}{\partial v}\right)_T > 0; \quad \left(\frac{\partial^2 p}{\partial v^2}\right)_T > 0 \tag{2.35}$$

According to J. Klein [KLEIN, 1974], the most impressive feature of the Van der Waals equation is the natural and inevitable way in which it accounts for the existence of the critical point, and for the disappearance of any distinction between liquid and gas above the critical temperature.

Any non-ideal gas, when compressed at sufficiently low temperatures, undergoes a

gas to liquid transition. The result of this transition is the condensation of gas into a liquid that occupies a significantly smaller volume. Van der Waals knew that the volume correction term used in his equation was just a approximation and could not be valid at high compressions. Although Van der Waals's model leads to inaccuracies as it approaches the critical point, its application is justifiable for qualitative studies.

The van der Waals equation of state is qualitatively reasonable and capable of describing the continuity between the liquid and vapor phases. Although Van der Waals equation of state (vdW EoS) has been shown to produce considerable errors for quantitative density prediction and any other related thermodynamic property, its work has given rise to the whole development of the study of non-ideal gases.

2.7 Peng-Robison Equation

In 1976 , Ding-Yu Peng and Donald B. Robinson [PENG; ROBINSON, 1970] worked together in a project for the Natural Gas Processors Association and proposed a new cubic equation of state (PR EoS). This new equation was the result of a change in the model presented by Redlich-Kwong, which was inaccurate for liquid density calculations and to predict other properties near the critical point. The proposed model for the Soave-Redlich-Kwong equation of state (SRK EoS) predicts a larger net volume than the experimental data. Much of this error can be explained by the fixed value compressibility factor for all gases ($Z_c = 1/3$). Based on empirical arguments, PR EoS changes the volumetric dependence by introducing the term (v-b), which improves the representation of the attractive pressure forces and predict better liquid densities.The PR EoS such as its derivatives is summarized in Table3

Table 3: Summary of Peng Robison equations of state

$$P = \frac{RT}{(v-b)} - \frac{a\,\alpha^2(T)}{v(v+b)+b(v-b)} \tag{2.36}$$

$$e(T,v) = c_v T - \frac{a\,\alpha(T)(\kappa+1)}{b\sqrt{2}}\, tanh^{-1}\frac{b\sqrt{2}}{v+b} \tag{2.37}$$

$$s(T,v) = c_v\, lnT + R\, ln(v-b) - \frac{a\,\alpha(T)\kappa}{b\sqrt{2\,T\,T_c}}\, tanh^{-1}\frac{b\sqrt{2}}{v+b} \tag{2.38}$$

$$a = 0.45724\,\frac{R^2T^2}{P_c^2} \qquad b = 0.0778\,\frac{R^2T^2}{P_c^2} \tag{2.39}$$

$$\alpha = 1 + \kappa\left(1 - \sqrt{\frac{T}{T_c}}\right) \tag{2.40}$$

where α is a dimensionless function of reduced temperature(T_r) and (ω) is often understood as a measure of the deviation of the molecular shape from a sphere. The PR EoS conserved the temperature dependency of the attractive term and the acentric factor introduced by Soave. The factor κ is a polynomial function of ω, $\kappa = \mathrm{f}(\omega)$.

The success achieved by Peng and Robison lies in assuming a more realistic value for the critical point compressibility factor ($Z_c = 0.307$), improving the thermodynamic predicts for hydrocarbons, considering the compression factor decreases as the carbon chain increase, improvement found by PR EoS is more evident for large molecules, although it works well for small molecules.

2.8 Peng-Robison Streak-Vera Equation

Peng-Robinson EoS became the most popular natural gas equation of state immediately after its publication. Naturally, this fact encourage anothers scientists to make modifications in order to improve it. In 1986, a important modification was made by Stryjek and Vera [STRYJEK; VERA, 1986], with the purpose to extend the applicability to low temperature regions.

Much of the effort of these two researchers focused on improving saturation pressure

prediction of up to 1.5 KPa for hydrocarbons. The qualitative cubic nature of the original EoS was preserved, but the reduced temperature (Tr) value was set at 0.7 and the κ value was reset to:

$$\kappa = \kappa_0 + \left[\kappa_1 + \kappa_2 \left((\kappa_3 - \sqrt{T_r})\right)\right] \left(1 + \sqrt{T_r})\right) (0.7 - T_r) \tag{2.41}$$

where κ_1, κ_2 and κ_3 are compound-specific adjustable parameters and κ_0 can be defined as

$$\kappa_0 = 0.378893 + 1.4897153\,\omega + 0.17131848\,\omega^2 + 0.0196554\,\omega^3 \tag{2.42}$$

The modified form of the Peng - Robinson equation, the PRSV equation, reproduces pure compound vapor pressures with accuracy better than 1% down to 1.5 kPa.

2.9 Thermo-physical numerical properties in SU2

In SU2 solver, the system of PDE equations that describes how mass, momentum and energy evolve in a control domain is usually written as:

$$\partial_t \vec{U} + \bigtriangledown . \vec{F^c} - \bigtriangledown . \vec{F^v} = \vec{Q} \;\; in \;\; \Omega, \;\; t > 0 \tag{2.43}$$

where $\vec{U}$ represents the the vector of conservative variables, ie. $\vec{U} = (\rho, \rho v_1, \rho v_2, \rho v_3, \rho E)^T$ and the vector $\vec{v}$ symbolizes the flow velocity, ie. $\vec{v} = (v_1, v_2, v_3) \;\epsilon\; R^3$, in a Cartesian coordinate system.

Numerical schemes for non-ideal fluid flows requires the calculation of partial derivatives of primary thermodynamics variables, thermodynamic properties as a function of density ρ and internal energy e, which are in turn a recombination of the conservative variables [PINI S. VITALE, 2017] as follows:

$$\rho = U_1, \quad e = \frac{U_5}{U_1} - \frac{(U_2 + U_3 + U_4)^2}{2{U_1}^2} = E - \frac{\left\|v^2\right\|}{2} \tag{2.44}$$

Any generic thermodynamic property X (pressure, temperature, etc.) can be determined using an arbitrary thermodynamic model,which is ensured by the stable equilibrium state principle, in the form:

$$X = X(\rho, v) = X(\vec{U}) \tag{2.45}$$

The Eq. 2.45 is explicit for polytropic models, like the Van der Waals (PvdW) and the Peng-Robinson Streak-Vera (iPRSV) available in SU2 thermodynamic library. The iPRSV EoS despite presenting inaccuracies near the critical point, is useful to initialize simulations where strong non-ideal flow effects are of concern. Therefore, this equation of state has become essential for this work.

3 PHISICAL MODELING

This chapter presents a state-of-the-art review of general properties of nucleation, with a particular focus on classical nucleation theory (CNT) and the Hill's Method of Moments. The review starts with an introduction to the field, briefly covering the physical principles of cluster nucleation and growth, and the main method of cluster formation. Finally, we close the review with a mathematical explanation of Hill's Method of Moments, another important tool used in our solver to obtain a quantitative analysis of the droplet population.

3.1 Supersaturation

Understanding the concept of supersaturation is essential to understanding the final droplet distribution during the nucleation process. While the undersaturated state and saturated state are thermodynamically stable, the supersaturated state is unstable. A supersaturated vapor in contact with the bulk liquid phase will condense onto the liquid until saturation is obtained.

Supersaturation is the inability of a fluid to condense when the saturated condition is reached in an expansion. Supersaturation is formulated in terms of the ratio of vapor pressure P and the saturation pressure corresponding to the local vapor temperature $P_s(T_v)$. This supersaturation can be defined by the equation below:

$$S = \frac{P}{P_s(T_v)} \tag{3.1}$$

3.2 Metastable State

In order to quantitatively describe metastable states, we need to define metastability. The concept of metastability was first introduced by works developed by Wilhelm Ostwald in 1897 and is the stability difference between the metastable state and equilibrium state at infinite size. Physically, a metastable state (supersaturated vapor) describes a phase in which an energy barrier must be surmounted before that phase can be transformed to one of lower energy.

According S. Cheng, [CHENG, 2008], since these supercooled or superheated non-equilibrium states are not at the lowest free energy for a specific temperature and pressure, they are thermodynamically defined as metastable and only exist for finite periods of time. In Fig. 6, the free energy (G) versus an order parameter (Φ) shows that the free energy height (ΔG^*) is the energetic activation barrier that a particle must overcome during the phase transition to reach equilibrium state.

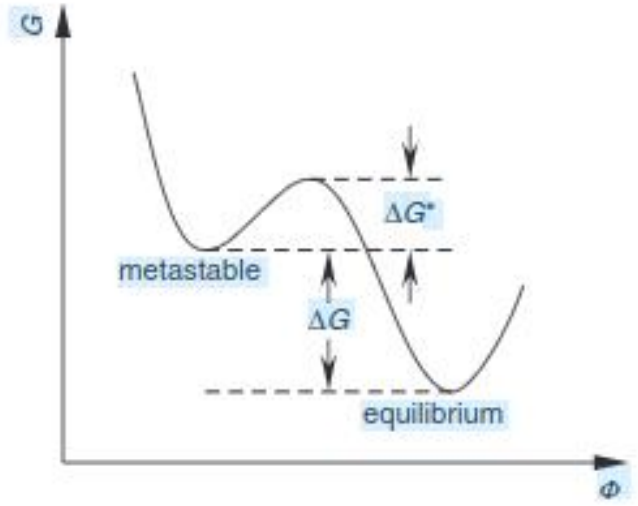

Figure 6: Representation of a metastable state using a plot of free energy (G) versus order parameter(Φ).
Source:[CHENG, 2008]

The difference between the two free energy (ΔG) represents the driving force for particle relaxation from the metastable state to the equilibrium state. The condensation of a gas phase is a classical example of a metastable state in the region between the binodal and spinodal curves, as shown in Fig.7. The spinodal curve is the limit of metastability and can be defined by the condition that the second derivative of Gibbs free energy is zero ($\partial^2 G/\partial\rho^2 = 0$). The local points of coexisting compositions, are known as binodal (coexistence) curve, and can be defined as when the first derivative ofthe Gibbs free energy

with respect to density is equal to zero ($\partial G/\partial \rho = 0$).

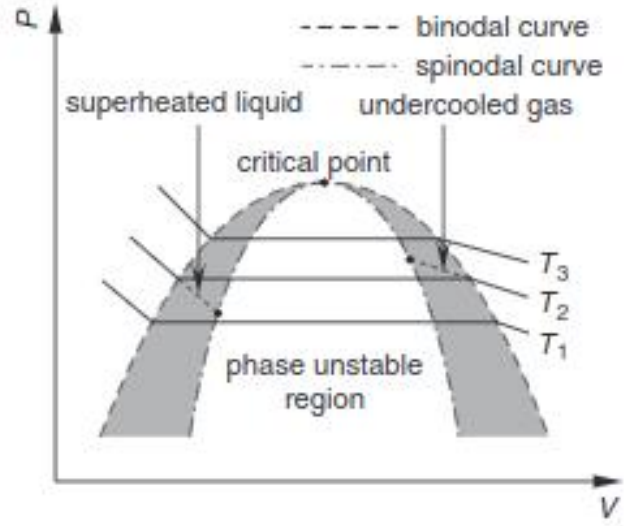

Figure 7: Illustration of the phase transition between the liquid and gas phases in a Pressure X Volume phase diagram
. Source: [CHENG, 2008]

3.3 The droplet growth

We can define nucleation as the kinetic processes involved at the beginning of a first-order phase transition, whereby a metastable phase becomes a more stable phase. The system can remain in the metastable state for a long time without transitioning to the most stable state until it is destabilized by changing an external parameter such as temperature or pressure. Thus, numerical models suitable for condensing flows under large temperature and pressure gradients, relevant for industrial applications, are complex and need to properly handle metastable thermodynamic states.

The first thermodynamic approach to the nucleation process is due the american scientist Josiah Willard Gibbs [GIBBS, 1875-1878], who demonstrated the dynamical theory of curved surfaces. Through his work, it became clear that reversible work required to form a new phase nucleus consists of a volumetric term and a superficial term. When a nucleus of sufficient size is formed, it tends to grow further until the supersaturation is relieved. The work required to form a single spherical droplet of radius in a supersatured vapour held at constant p and T can be broken down in to some steps. First , a isothermal expansion of the vapour:

$$\Delta G_1 = \frac{4}{3}\pi r^3 \rho_L \int_p^{p_{S(T_G)}} \frac{1}{\rho_G} dp \tag{3.2}$$

Using a truncated virial series, we can model the gas behavior not ideal for high pressures:

$$\Delta G_1 = \frac{4}{3}\pi r^3 \rho_L R T_G \left[ln\frac{\rho_G}{\rho_{GS}} + 2B(\rho_{GS} - \rho_G) + \frac{3}{2}C(\rho_{GS^2} - \rho_{G^2}) + \frac{4}{3}D(\rho_{GS^3} - \rho_{G^3}) \right] \tag{3.3}$$

where B,C and D are the second, third and fourth virial coefficients respectively. At constant temperature and pressure $p_S(T_G)$, the condensation of vapour to bulk liquid will be:

$$\Delta G_2 = 0 \tag{3.4}$$

The isothermal compression of liquid to pressure p gives:

$$\Delta G_3 = \frac{4}{3}\pi r^3 \ [\, p - p_S(T_G)\,] \tag{3.5}$$

The ΔG_3 is small and can be neglected . The formation of a droplet of radius r can be express:

$$\Delta G_4 = 4\pi r^2 \sigma \tag{3.6}$$

where σ is the surface tension. The Eq.3.6 is the capillarity approximation. The sum of all free energy terms gives the reversible work required to form a single spherical droplet:

$$\Delta G = \overbrace{4\pi r^2 \sigma}^{1} + \underbrace{\frac{4}{3}\pi r^3 \rho_L R\, T_G\, ln\, S}_{2} \tag{3.7}$$

where ρ_L is the liquid density, σ is the surface tension, $S = p/p_s(T_G)$ is the supersaturation ratio being the saturation vapour pressure at T_G. The term represented by the number 1 in brackets, will always be positive but the other term (2) in the equation, will be negative for supersaturated vapors ($S > 1$). The Fig. 8 show the variation of with r for superheated ($S < 1$) and supersaturated vapour ($S > 1$).

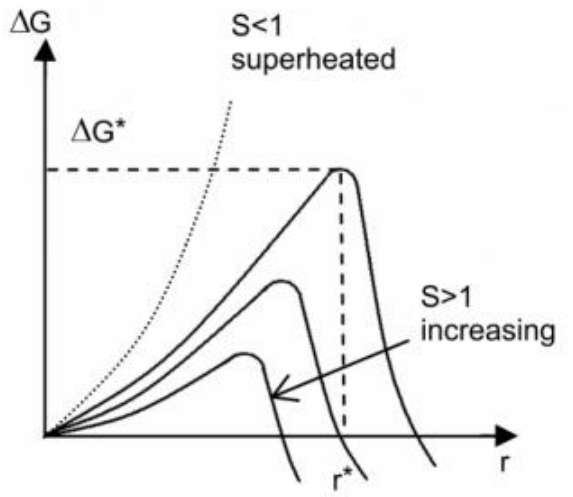

Figure 8: Variation of the Gibb's free energy for various supersaturation ratios. Source: [FAKHARI, 2017]

Looking at Fig.8, we can conclude that the value of ΔG increases proportionally to the radius (r) up to a maximum value ΔG^*. At this point, the droplet radius reaches its maximum value, known as the critical radius (r^*). A droplet with $r > r^*$ can reduce the free energy of system and has a tendency to grow.

We can get the expression for the critical radius by differentiating Eq. 3.9 with respect to r and equaling to zero:

$$r^* = \frac{2\sigma}{\rho_L R T_G ln S} \tag{3.8}$$

Substituting Eq. 3.8. into Eq. 3.9, we will have the expression for ΔG^* :

$$\Delta G^* = \frac{16\pi\sigma^3}{3(\rho_L R\, T_G\, ln\, S)^2} \tag{3.9}$$

3.4 The Nucleation Theory

The groundwork for the theoretical nucleation theory, was developed by the works of Volmer and Weber [VOLMER, 1925], using a statical-thermodynamic approach. By treating the nucleation barrier as activation energy, on the basis of Boltzmann's relationship

between entropy and probability , Volmer wrote:

$$J = A\ exp\left(\frac{-\Delta G^*}{k_B T}\right) \tag{3.10}$$

where A is a pre-exponential factor, k_B is the Boltzmann constant and the nucleation rate (J) describes how many nuclei of critical size form on a substrate per unit area/time.

3.4.1 The Classical Nucleation Theory

The success of Volmer's work has encouraged many other researchers to contribute to the improvement of this classic equation. The Classical Nucleation Theory (CNT) assumed that liquid droplets are all spherical and that the vapor phase and liquid phase have the same temperature and can be written as follows

$$J_{CNT} = q_c \frac{\rho_v^2}{\rho_l}\left(\frac{2\sigma}{\pi m^3}\right)^{1/2} \exp\left(-\frac{4\pi r_c^2 \sigma}{3k_B T_v}\right) \tag{3.11}$$

where q_c is the condensation coefficient , ρ_v is the density of the vapor phase, ρ_l is the density of the liquid phase and m is the mass of a molecule.

The simplicity surrounding this theory has made possible to rationalize experimental measurements and to describe the stage of nucleation in the mesoscopic modeling of phase transformations. Although the CNT failed to predict it accurately. Therefore several corrections have been proposed to this theory.

3.4.2 Non-Isothermal correction

One of the corrections, proposed by Kantrowitz, to the CNT is the non-isothermal correction, which drops the assumption that the vapor and liquid phases have the same temperature. The non-isothermal nucleation rate is given by:

$$J_{NonIso} = \left(\frac{1}{1+\phi}\right) q_c \frac{\rho_v^2}{\rho_l}\left(\frac{2\sigma}{\pi m^3}\right)^{1/2} \exp\left(-\frac{4\pi r_c^2 \sigma}{3kT_v}\right) \tag{3.12}$$

where ϕ is given by:

$$\phi = q_c \frac{\rho_v R}{\alpha_r} \sqrt{\frac{RT_v}{2\pi}} \frac{H_e}{RT_v} \left(\frac{H_e}{RT_v} - \frac{1}{2} \right) \tag{3.13}$$

where, H_e is the specific enthalpy of evaporation and α_r is the surface heat transfer coefficient of a droplet whose radius is equal to the critical radius r_c.

3.4.3 Internally Consistent Classical Theory (ICCT)

Another nucleation rate model is the one proposed by the Internally Consistent Classical Theory (ICCT). According to [HALAMA, 2012] it is given by:

$$J_{ICCT} = 0.01 \frac{q_c}{S} \frac{\rho_v^2}{\rho_l} \left(\frac{2\sigma}{\pi m^3} \right)^{1/2} \exp\left(\frac{\sigma a_0}{kT_v} \right) \exp\left(- \frac{4\pi r_c^2 \sigma}{3kT_v} \right) \tag{3.14}$$

where S is the supersaturation rate and a_0 is given by:

$$a_0 = (36\pi)^{1/3} \left(\frac{m}{\rho_l} \right)^{2/3} \tag{3.15}$$

where m is the mass of a molecule, and ρ_l is the liquid density.

3.5 Hill's Method of Moments

To explain Hill's Method of Moments let's assume that in a small volume (V),contains a mixture consisting of an inert gas and a vapor (air / water mixture), assuming that the inert gas will not condense. By the law of conservation of mass we will have:

$$M = M_a + M_v + M_l \tag{3.16}$$

where M is the total mass in the control volume, M_a is the mass of inerte gas, M_v is the mass of condensible substance in gaseous form and M_l is the mass of substance in liquid form. In order to facilitate some calculations in the future we will use a dimensionless liquid mass fraction (g):

$$g = \frac{M_l}{M} = \rho_l \frac{V_l}{\rho V} \qquad 0 < g < g_{max} \tag{3.17}$$

the dimensionless liquid mass fraction is dependent of time, and consequently, the volume occupied by the liquid V_l, the total volume V and the density of the complete mixture ρ (vapour and liquid) . So we will have:

$$g(t) = \rho_l \frac{V_l(t)}{\rho(t)V(t)} \tag{3.18}$$

In order to find the volume occupied by the liquid portion, we must integrate the term V_l:

$$V_l = \int_0^t \frac{4}{3}\pi r^3(t,\tau)J(\tau)V(\tau)d(\tau) \tag{3.19}$$

where the function $r(t,\tau)$ describes the formation of the droplet radius from the beginning , $V(\tau)$ is the size of control volume at the moment of nucleation, $J(\tau)$ is the nucleation rate per unit volume and $\frac{4}{3}\pi r^3$ is the volume of droplets (assuming that all the droplets have the shape of a sphere). Thus:

$$g(t) = \rho_l \frac{\int_0^t \frac{4}{3}\pi r^3(t,\tau)J(\tau)V(\tau)d(\tau)}{\rho(t)V(t)} \tag{3.20}$$

We can assume that the drops do not move relative to the surrounding gas mixture, known as the non-slip condition in the Hill Moment Method.

$$dM = 0 = M = p(\tau)V(\tau) = p(t)V(t) \tag{3.21}$$

Knowing that the function $r(t,\tau)$ is not available in closed form, we must replaced the droplet growth rate in its closed form dr/dt. The liquid mass fraction now becomes differentiated with respect to time:

$$\frac{dg}{dt} = \rho_l \int_0^t \frac{4}{3}\pi r^3(t,\tau)\frac{J(\tau)}{\rho(\tau)}d\tau \tag{3.22}$$

after some mathematical manipulations we will have :

$$\frac{dg}{dt} = \rho_l \frac{4}{3}\pi r^{*3}\frac{J(\tau)}{\rho(\tau)} + 3\rho_l \int_0^t \frac{4}{3}\pi r^3(t,\tau)\frac{dr(t,\tau)}{dt}\frac{J(\tau)}{\rho(\tau)}d\tau \tag{3.23}$$

at this point we should do some simplifications : The droplet growth rate [$\frac{dr}{dt}$] is independent of the initial droplet radius.This simplification is true for larger radius droplets but does not apply to droplets that have a very small radius due to surface tension dependence.

$$\frac{dr}{dt} \neq \frac{dr}{dt}(r(t,\tau)) \tag{3.24}$$

the droplet growth rate can be written:

$$\frac{dr}{dt} = \frac{dr}{dt}(t) \tag{3.25}$$

Now we can calculate the change in radius with time outside the integral:

$$\frac{dg}{dt} = \underbrace{\rho_l \frac{4}{3}\pi r^{*3} \frac{J(\tau)}{\rho(\tau)} + 3\frac{dr}{dt}(t)\rho_l}_{2} \overbrace{\int_0^t \frac{4}{3}\pi r^n(t,\tau)\frac{J(\tau)}{\rho(\tau)}d\tau}^{1}$$

It is important to pause and analyze the new equation above. The bracket part (1) represents the original integral, but with the radius power reduced by one unit and multiplied by the droplet growth rate. It is interesting to introduce the concept of liquid moment, as follows:

$$Q_n(t) = \int_0^t r^n(t,\tau)\frac{J(\tau)}{\rho(\tau)}d\tau \tag{3.27}$$

Developing the expression of liquid moment as a function of time:

$$\frac{dQ_n(t)}{dt} = r^n(t)\frac{J(t)}{\rho(t)}dt + n\frac{dr}{dt}(t)Q_{n-1} \tag{3.28}$$

We can describe the formulation of liquid moments as follows:

$$Q_0 = \int_0^t \frac{J(\tau)}{\rho(\tau)}d\tau \tag{3.29}$$

$$Q_1 = \int_0^t r(t,\tau)\frac{J(\tau)}{\rho(\tau)}d\tau \tag{3.30}$$

$$Q_2 = \int_0^t r^2(t,\tau)\frac{J(\tau)}{\rho(\tau)}d\tau \tag{3.31}$$

$$Q_3 = \int_0^t r^3(t,\tau)\frac{J(\tau)}{\rho(\tau)}d\tau \tag{3.32}$$

We should pause again and go back to Eq. 3.22. Looking closely, we can see that the liquid moment Q_3 is closely related to the liquid mass fraction:

$$g(t) = \rho_l \frac{4}{3}\pi Q_3(t) = \frac{dg(t)}{dt} = \rho_l \frac{4}{3}\pi \frac{dQ_3(t)}{dt} \tag{3.33}$$

The first moment Q_0 does not have a time dependency on its integral. By differentiating this first moment we have:

$$\frac{dQ_0}{dt} = \frac{d}{dt}\left(\int_0^t \frac{J(\tau)}{\rho(\tau)}d\tau\right) = \frac{J(t)}{\rho(t)} \tag{3.34}$$

We conclude that there is no closure to the solution of the set of moments, since the logical expansion defined by the recurrence relation for the liquid moments is not continued to $n < 0$. Therefore, the system of ordinary differential equations becomes:

$$\frac{dQ_0}{dt} = \frac{J(t)}{\rho(t)} \tag{3.35}$$

$$\frac{dQ_1}{dt} = r^*\frac{J(t)}{\rho(t)} + \frac{dr(t)}{dt}Q_0 \tag{3.36}$$

$$\frac{dQ_2}{dt} = r^{*2}\frac{J(t)}{\rho(t)} + 2\frac{dr(t)}{dt}Q_1 \tag{3.37}$$

$$\frac{dQ_3}{dt} = r^{*3}\frac{J(t)}{\rho(t)} + 3\frac{dr(t)}{dt}Q_2 \tag{3.38}$$

By rewriting the system of ordinary differential equations described above, by addition of the product of vector Q and the continuity equation for mass, we will obtain a set of equations that will provide the integral properties of the droplet distribution:

$$\frac{\partial \rho Q_0}{\partial t} + \frac{\partial \rho Q_0 u_i}{\partial x_i} = J(t) \tag{3.39}$$

$$\frac{\partial \rho Q_1}{\partial t} + \frac{\partial \rho Q_1 u_i}{\partial x_i} = r^* J(t) + \frac{dr}{dt}(t)\rho Q_0 \tag{3.40}$$

$$\frac{\partial \rho Q_2}{\partial t} + \frac{\partial \rho Q_2 u_i}{\partial x_i} = r^{*2} J(t) + 2\frac{dr}{dt}(t)\rho Q_1 \tag{3.41}$$

$$\frac{\partial \rho Q_3}{\partial t} + \frac{\partial \rho Q_3 u_i}{\partial x_i} = r^{*3} J(t) + 3\frac{dr}{dt}(t)\rho Q_2 \tag{3.42}$$

where u_i is the velocity components in spatial and x_i is the the spatial coordinates.The droplet growth rate are no longer defined as a function of the spatial gradients of the flow domain. Finally the new equation for the liquid mass fraction will be:

$$g(t) = \rho_l \frac{4}{3}\pi Q_3(t) = \frac{dg(t)}{dt} = \rho_l \frac{4}{3}\pi \frac{(\rho Q_3(t))}{\rho} \tag{3.43}$$

The zeroth order moment is the total number of liquid droplets per unit mass of mixture. The first order moment is related to the average droplet radius, the second order moment is related to the total droplet surface area, and the third order moment is related to the wetness fraction. Hill defined the radius needed for droplet growth laws as:

$$r_H = \sqrt{\frac{Q_2}{Q_0}} \tag{3.44}$$

The growth rate model that was proposed by Hill is given by:

$$\left.\frac{dr}{dt}\right|_H = \frac{P_v}{\rho_l H_e \sqrt{2\pi R T_v}} \left(\frac{\gamma + 1}{\gamma}\right) C_p^v (T_s(P) - T_v) \tag{3.45}$$

Where C_p^v is the vapor phase specif heat at constant pressure, γ is the specific heat ratio, R is the gas constant, P_v is the vapor pressure, ρ_l is the liquid density, H_e is the specific enthalpy of evaporation, T_v is the vapor temperature, and $T_s(P)$ is the saturated vapor temperature at pressure P.

The great advantage of nucleation-coupled models, such as moment models, is in the fact that easily executed on a microcomputer due the low computational cost.

4 NUMERICAL RESULTS

The previous chapters have presented the basic considerations on the set of thermodynamic state equations, the classical condensation theory (CNT) and that were considered for this work. This chapter presents the integration of theses parts, through numerical results, validated with experimental data available in the literature.

4.1 Numerical Methodology

The solver SU2 was used for the calculations of the two-phase flow in the nozzle [VITALE et al., 2015]. The SU2 suite is an open-source collection of C++ based software tools for performing Partial Differential Equation (PDE) analysis and solving PDE-constrained optimization problems. The software has been developed to solve multiphysics analysis and optimization tasks using unstructured mesh topologies. A detailed description of the numerical methodology can be found in APPENDIX A .

The advantage of working with an open-source code is not only that it allows us the possibility of implementing new algorithms and thus contribute to the development of the code but it also gives us access to the full code. The numerical approach is based on a finite-volume method using an implicit, compressible formulation with a second order spatial discretization. The onset of nucleation is defined through classical nucleation theory under the assumptions of non-equilibrium and homogeneous condensation.

4.2 Mesh generation

The mesh generation in 2D and 3D is a real challenge due to the complex characteristics and phenomenas at various scales that a flow may have: boundary layers, shock waves and turbulence. Clearly to capture such phenomenas, the researcher must choose a robust and reliable mesh generator. All meshes of this work were generated using the GMSH 4.5 software [GMESH, 2019], the open source 3D finite element mesh generator

and the built-in CAD engine.

4.3 Non-Ideal Gas Investigation

Today, the most sophisticated CFD codes present many tools for performing viscous flow numerical simulations involving non-ideal compressible fluids (NICFD). However, the correct prediction of some phenomena such as condensation is still an arduous and demanding task, and the results are not always in accordance with the physics of the problem. Due to the complexity surrounding the behavior of non-ideal gases, the success of such simulations depends on robust and properly validated codes.

4.3.1 TEST CASE A: Arina's Nozzle

Our approach to the condensation problem was initially to study and model a simple case (without condensation) and then gradually increase the complexity of our models. Our computational method in supersonic flows was validated with Arina's results. First, we simulated the flow of air, using the ideal gas equation of state (EoS) and an inviscid (Euler) model. Then we proceeded to a more sophisticated model considering the flow of CO_2 in a three dimensional Arina nozzle, using an non-ideal equation of state, the Peng-Robinson EoS, and considering the viscous effects and also using a turbulence model, the k-ω SST.

The Arina's geometry can be seen in appendix B and the set of boundary conditions for the simulations are summarized in Table 4.

Table 4: Flow parameters and boundaries conditions for a Test Case A.

Fluid	CO_2
Physical Problem	Navier Stokes
Turbulance Model	SST
Equation of State	PRSV
Gas Constant	118.92(J/Kg*K)
Specific heat ratio	1.29
Critical Temperature	304.18 K
Critical Pressure	$7380000 N/m^2$
Critical density	467 kg/m^3
Inlet Total Pressure	1 bar
Inlet Total Temperature	300 K
Static outlet pressure	0.83 bar
Spatial scheme	ROE - $1°order$

The entropy for the Navier-Stokes turbulent flow of pure CO_2 is shown in Figures 9 and 10.

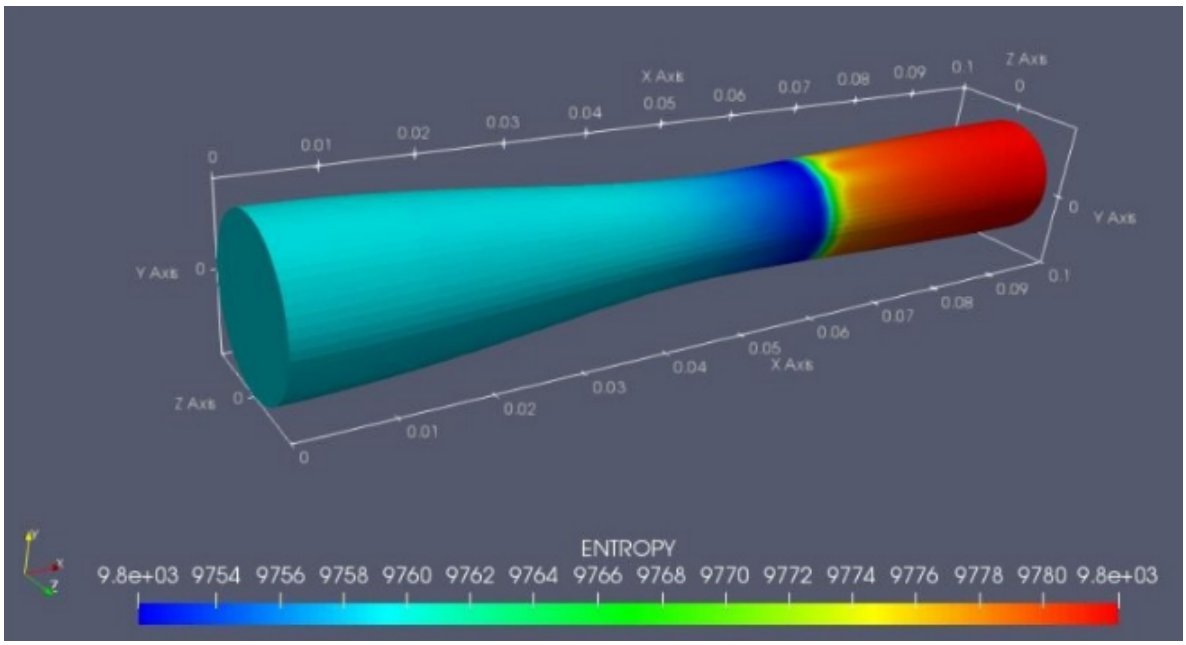

Figure 9: Entropy for the Navier-Stokes turbulent flow using CO_2 as fluid.
Source: Author

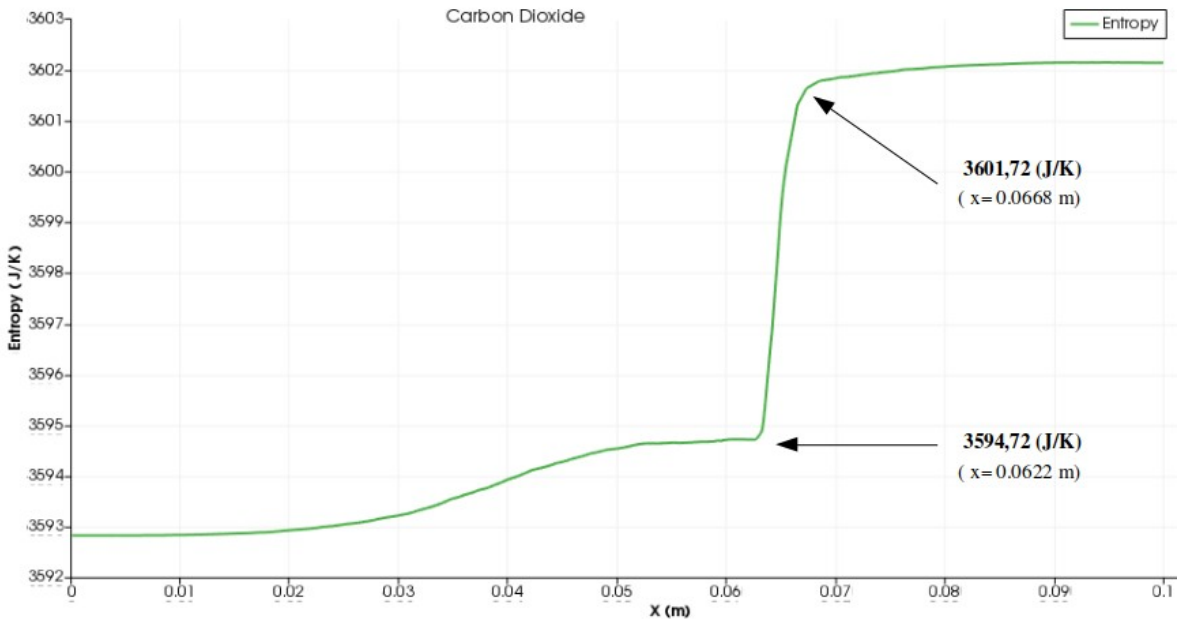

Figure 10: Entropy profile along x-axis: CO_2.
Source: Author

The entropy is an important aspect that helps us to verified the model. In this case, we see that the entropy increases after the normal shock wave, which is consistent with the physics of the problem. Also, the inviscid (Euler) model will show constant entropy with an increase in it only after the shock wave. The viscous (Navier-Stokes) model, however, shows a variation of entropy along the nozzle and an increase in it after the shock wave. This is consistent with the physics of the problem and occurs due to the action of viscous dissipation. Another important aspect to verified the model is the stagnation enthalpy, shown in Fig.11 , which should remain constant throughout the flow. We can see that the stagnation enthalpy is constant except in the shock wave where there is a small variation, which is expected since in the shock wave there is a discontinuity in thermodynamic properties.

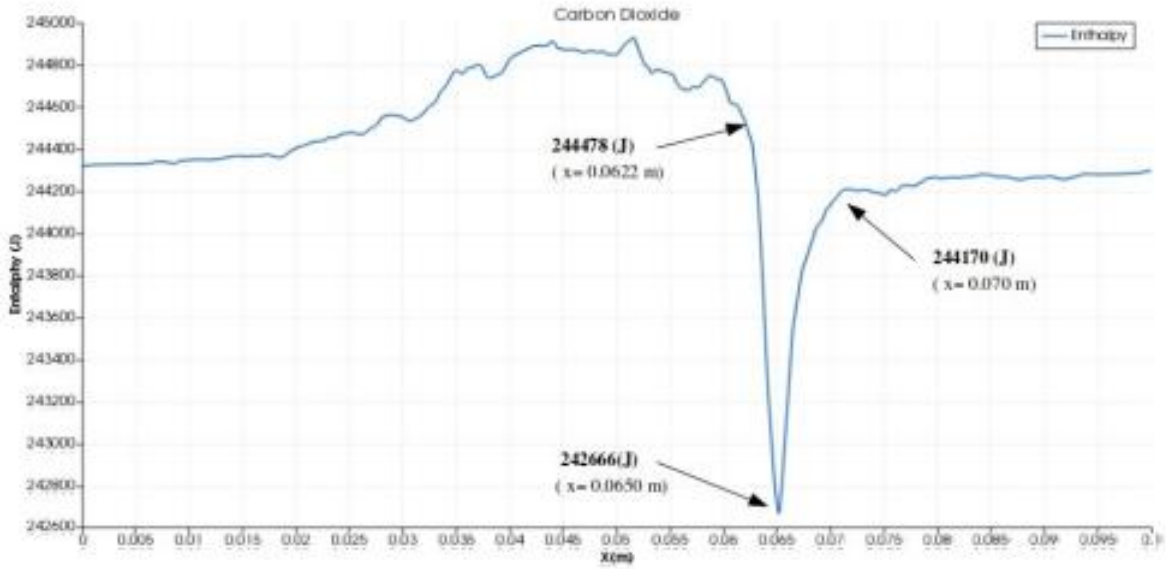

Figure 11: Enthalpy profile along x-axis: carbon dioxide.
Source: Author

Observing all figures shown above, the numerical results obtained agree with the literature, numerically validating the nozzle. Despite the great contribution made by Arina [ARINA, 2004], his work is essentially numerical and has no experimental data for the condensation phenomenon 's validation.

4.4 Condensation investigation

The initial validation of wet-steam methods relies heavily on experimental data obtained from condensing nozzle flows. Many tests involving nozzles have been performed in order to understand the phenomenona. However, Binnie and Grenn [BINNIE, 1941] and Moses and Stein [MOSES, 1978] are the most popular tests for reliable validations.In this subsection, the results of our model are compared with the experimental data reported in literature with existing numerical solutions obtained with numerical methods.

4.4.1 TEST CASE B: Binnie and Green 's nozzle

Two tests were conducted on Binnie and Green nozzle for wet steam flow conditions. The calculation was made using a branch ("feature-turbo2phase") of the CFD code Stanford University Unstructured (SU2), which was developed by researches from TU Delft. This branch is still under development and in order to contribute to the advancement of this work, an investigation was conducted to identify the capabilities and limitations of

the code, as well as its accuracy in predicting the position of the condensation wave.

The condensation model available on the branch was the Classical Nucleation Theory (CNT). It calculates the CNT nucleation rate with the non-isothermal correction which according to the literature produces more accurate results. In our simulations we used the two-dimensional Euler equations, the Peng-Robinson Stryjek Vera (iPRSV) equation of state and a mesh of approximately 55000 elements. Reference Binnie et al. provides experimental results for low-pressure condensation of water vapor.

We have found out that the code was able to successfully reproduce the physics of condensation (after introducing a correction factor that will be explained in the next sub-section), i.e., the release of latent heat that occurs during the phase change and the increase in static pressure where condensation takes place commonly referred to as the condensation wave. Also, due to the increase in pressure there is a reduction in the Mach number, which the code was also able to predict. A total of two cases were simulated with the code and compared with the experimental data of Binnie et al. [BINNIE, 1941]. The cases and the conditions used in each one of them are shown in table 5.

Table 5: Numerical setup for a Test Case B.

Case	P_0 (Bar)	T_0 (K)
95	0.6550	370
92	0.6550	400

The total pressure was kept constant throughout the experiment, while the static inlet temperature was varied. The pressure and Mach number profiles obtained by simulation using SU2 solver (for case 92) are shown in Fig. 12.

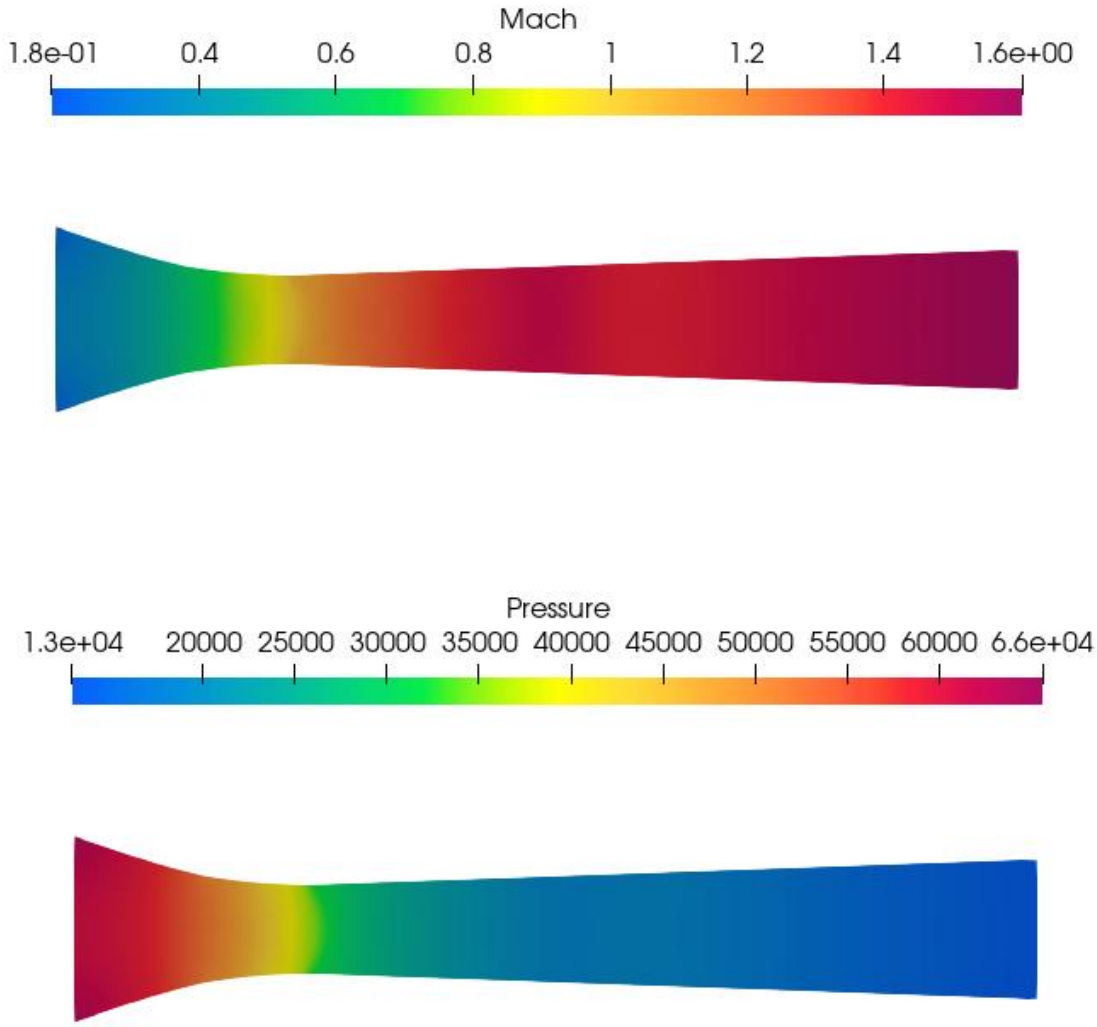

Figure 12: Pressure and Mach number profiles for case 92.
Source: Author

The Fig. 13 shows the results for sets of experiments performed Binnie and Green. The Fig.14 presents the numerical results for static pressure obtained for cases 92 and 95 (respectively indicated by the red arrows). By comparing the pressure profiles of cases obtained by experimental data , it is evident that the condensation waves were successfully captured.

A small difference in waves 's positions may be noted, but we must remember that viscous effects are not being considered. Another important factor is the inaccuracy of the CNT nucleation model to capture the condensation wave,

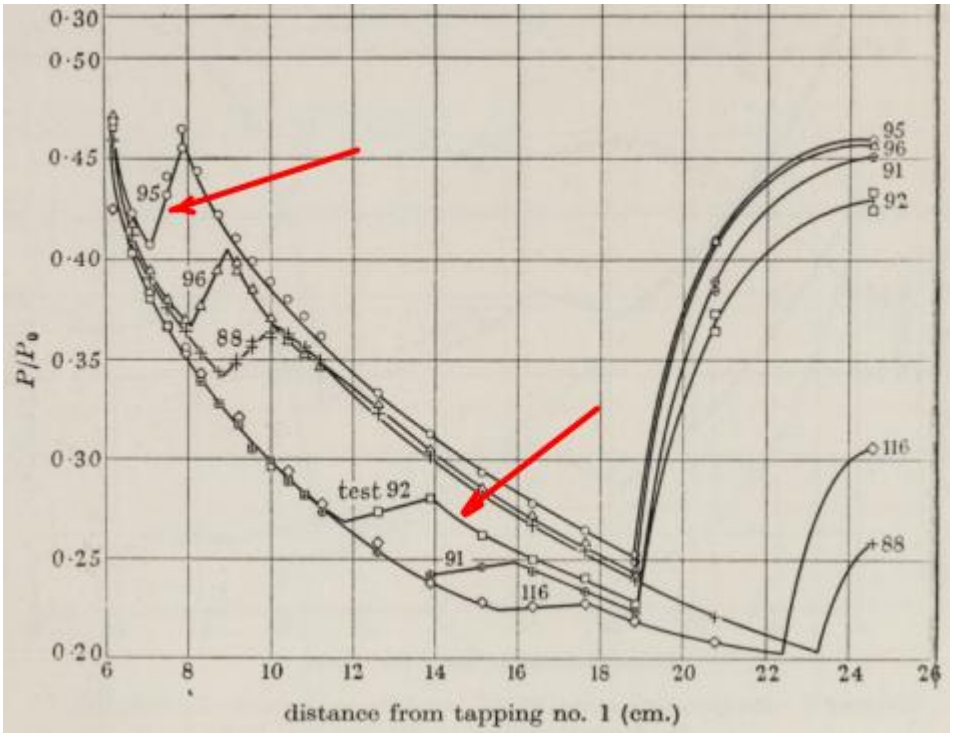

Figure 13: Comparison of pressure distribution for various flow conditions along then Binnie's nozzle.
Source: [BINNIE, 1941]

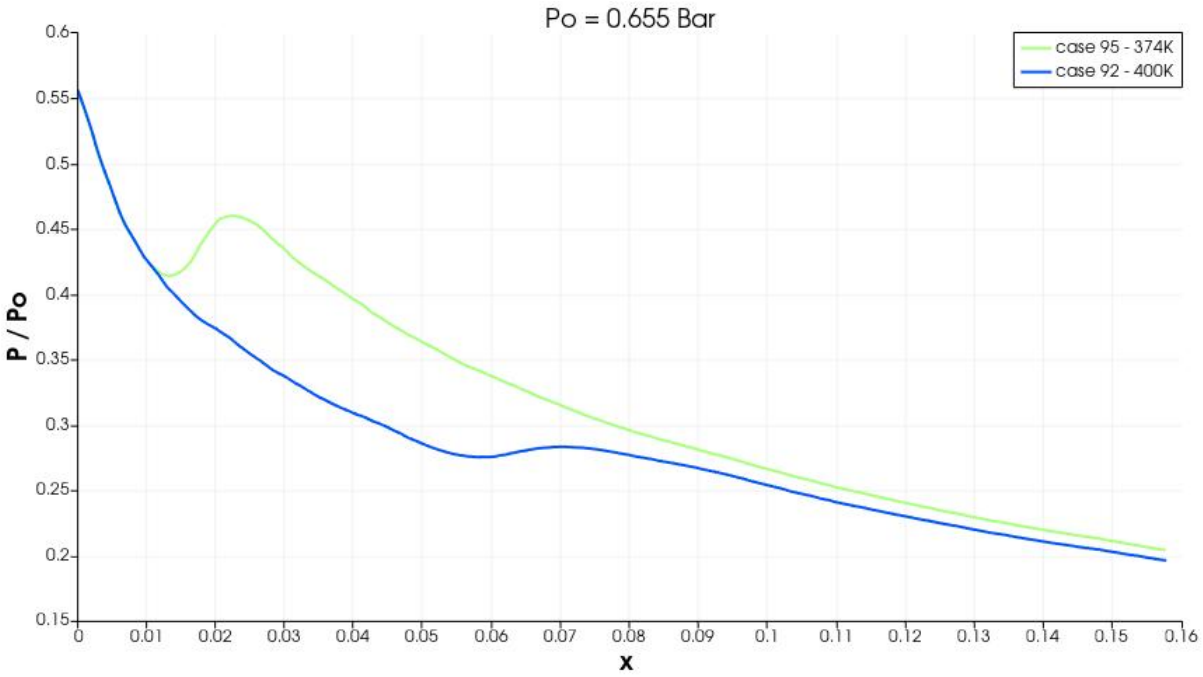

Figure 14: Numerical results obtained with SU2 solver for Binnies and Green 's cases.
Source: Author

It is important to note the influence of the inlet static temperature on the conduction wave position, keeping the total pressure constant. By increasing the temperature, the wave will occur downstream of the throat.

4.4.2 TEST CASE C: Moses and Stein nozzle

The well–known Moses and Stein nozzle, which is a representative study of supersonic wet-steam flows, was used in Test Case C. The shape of the profile is reported in Appendix A. All the calculations are performed on a 50000 cells grid. Pressure measurements and a light-scattering method was used to obtain droplet size data along the nozzle centre.

Due to the wide range of pressures and temperatures investigated, this work was of great importance for the numerical investigations performed by this research. The Fig. 28 shows the results for sets of experiments performed, keeping the inlet pressure fixed($P_0 = 39996,7$ Pa) while varying the inlet temperature. The ordinate axis represents the ratio of the static pressure to the total pressure used in the experiment, while the abscissa axis represents the distance from the nozzle, starting exactly where the pressure gauges were fixed downstream of the throat (x = 8 cm).

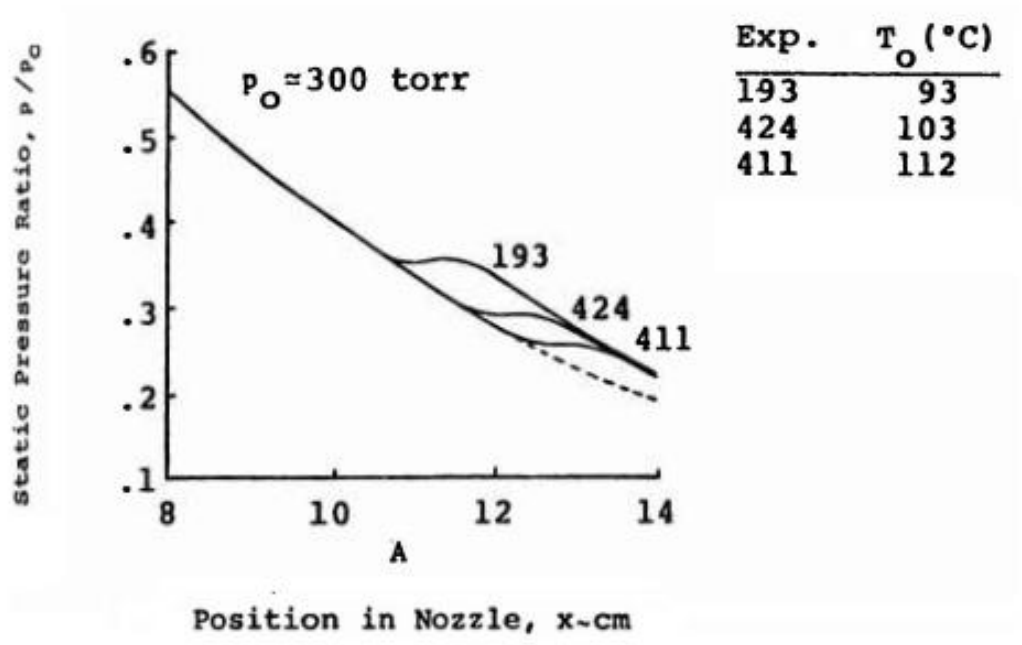

Figure 15: Comparison of pressure distribution for various flow conditions along the nozzle.
Source: [MOSES, 1978]

For modeling the low-pressure condensation vapor flow in this nozzle, in addition to the mandatory Euler equations, the Kantrowitz non-isothermal nucleation model, described in Eq. 3.13, was used to determine the droplet formation. The set of boundary conditions for the simulations are summarized in Table **??**.

Table 6: Flow parameters and boundaries conditions for a Test Case C.

Fluid	H_2O
Physical Problem	EULER
EoS	iPRSV
Gas Constant	461.51(J/Kg*K)
Specific heat ratio	1.29
Critical Temperature	647.12 K
Critical Pressure	$22060000 N/m^2$
Critical Density	322 Kg/m ^{3}
Inlet Total Pressure	39996,71 Pa
(Exp.193)- Inlet Total Temperature	363,15 K
(Exp.411)- Inlet Total Temperature	385,15 K
(Exp.424)- Inlet Total Temperature	376,15 K
Static outlet pressure	9999.175 Pa
Spatial scheme	ROE - $1°order$

The Fig. 16 presents the static pressure obtained for cases 193, 411 and 424. For case 424, a flow without condensation was simulated and another with the presence of condensation for didactic purposes. The condensation wave was successfully captured and we can see that as the temperature rises, the position of the condensation wave occurs downstream of the nozzle.

Firstly, it is noteworthy that even upstream of condensation, the numerical results clearly differ from the original test cases. The Fig.17 shows the position difference between the experimental data and the numerical results obtained with the SU2 solver for case 193.The challenge of numerically reproducing the exact point where the condensation wave occurs occurs mainly depends on the accuracy of the nucleation rate equation used.

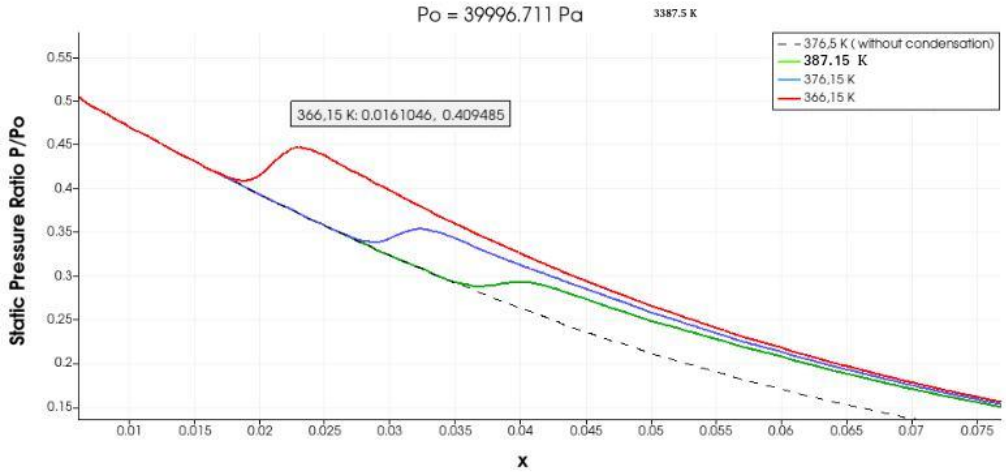

Figure 16: Numerical results obtained with SU2 solver for Moses and Stein 's cases . Source: Author

	Starting Conditions		Onset condensation	
Exp	Total Pressure (Pa)	Temperature (K)	Position (cm)	Static Pressure (Pa)
193	39996.71	366	10.74	14798.7

	Starting Conditions		Onset condensation	
SU2	Total Pressure (Pa)	Temperature (K)	Position (cm)	Static Pressure (Pa)
193	39996.71	366	9.853	16378.4

Figure 17: Numerical onset condensations position compared to experimental data. Source: Author .

Moreover, the discrepancy could be partly explained by the different average definition. In the CFD simulations, the radius droplet represents a volume averaged, whereasin the experiment another approach is used (the Sauter mean radius). A another reason for this incorrectly result is that the droplet growth model that was being used inside solver, without proper corrections, resulting in a lower droplet growth than the results obtained by the experiments.

Recent research advises that Young's growth model [YOUNG, 1992] is most appropriate for this purpose

Unfortunately, both droplet growth models result in a late prediction of the condensation pressure rise, reflecting the relatively slow growth rate. In order to improve the accuracy of droplet growth formulation, Marius Grübel, Markus Schatz and Damian M. Vogt [GRUBEL J. STARZMANN; VOGT, 2018] concluded that a correction factor (f= 1.33) should be introduced to Young's growth model. The author of this dissertation changed the primary code within SU2 and introduced (among other modifications) the new equation below:

$$J_f = \frac{q_c}{1+\varepsilon}\frac{\rho_v^2}{\rho_l}\left(\frac{2\sigma}{\pi m_m^3}\right)^{1/2} exp\left(-f\frac{4\pi\sigma r^{*2}}{3k_B T_v}\right) \tag{4.1}$$

The Fig. 18. presents the results after introducing the correction factor into the SU2 solver code for case 193.

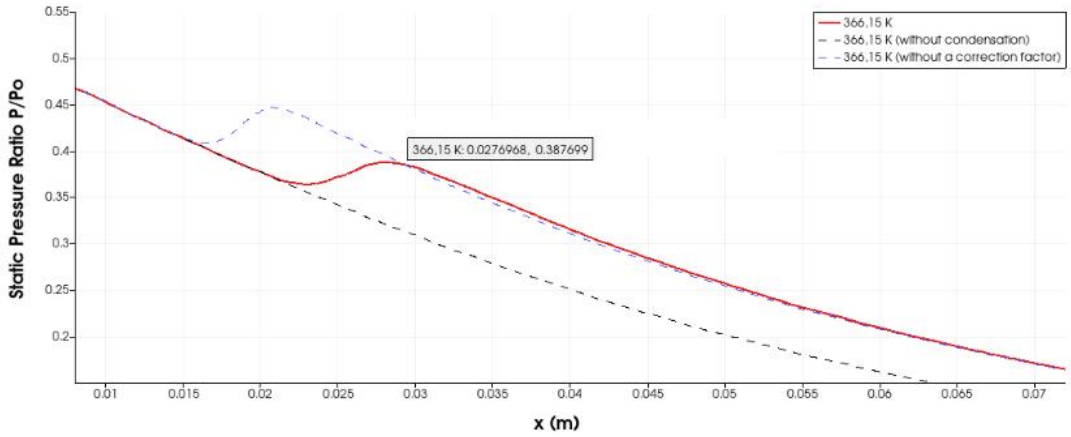

Figure 18: Numerical results obtained with SU2 solver with correction factor applied. Source: Author

The blue dashed line represents case 193 without the correction factor, with the condensation wave occurring upstream of the nozzle. The new simulation, represented by the red line, shows that the correction factor (f) captured the condensation wave very close to the point obtained by the experiments of Moses and Stein. According to Grübel, there is no physical explanation for this factor yet, being totally empirical, based on several experiments.

It is important to note that, initially, the branch *feature-turbo2phase* had only the

classic nucleation rate model (CNT). The author introduced two other models in the code: Internally Consistent Classical Theory (ICCT) and the correction factor *f*.

For the purpose of illustration, Fig.19 shows a comparison of the results obtained for each nucleation rate model. The simulations were based on experiment 424 (represented by the red dots) from the studies by Moses and Stein, and through a quick analysis it is clear that the new nucleation rate models implemented are more accurate than the classic model (CNT). The correction proposed by Internally Consistent Classical Theory (ICCT) ,represented by the dotted green line, increases the accuracy of the capture of the condensation wave.

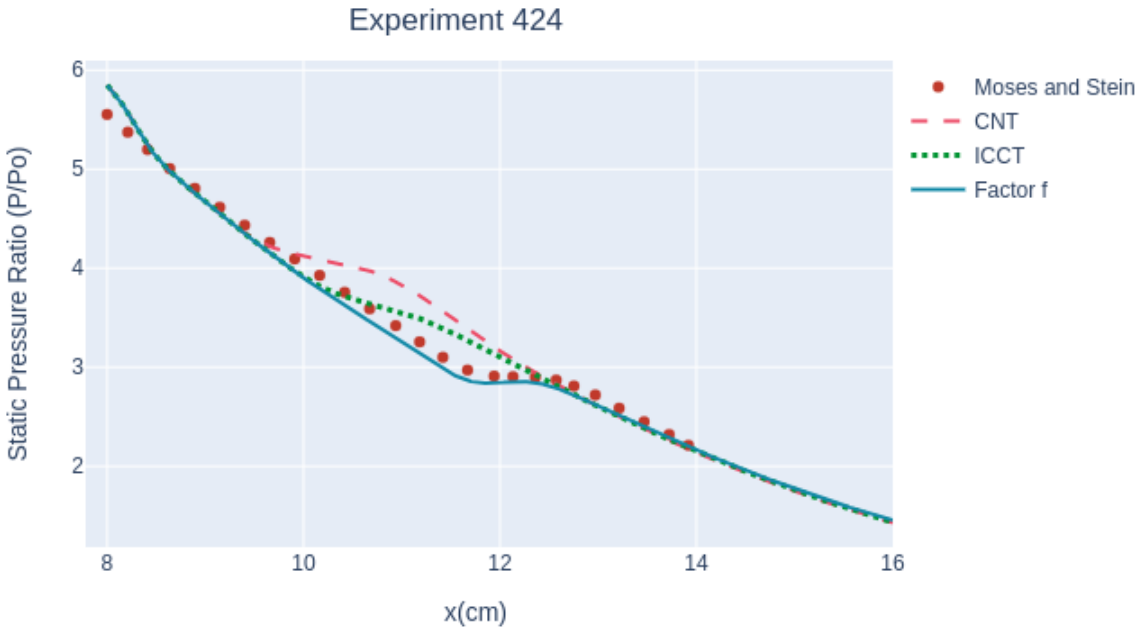

Figure 19: Comparison of the Static Pressure ratio along the nozzle,for different nucleation models.
Source: Author

Although the ICCT model shows significant improvements over the CNT model, it still overestimates the value of the droplet population, as can be seen in Figure **??**. We can observe that for the CNT model, nucleation starts upstream at point x = 9.256 cm, while for the ICCT model, nucleation starts downstream at point x = 9.688 cm. The numerical values of both models for the zeroth order moment are not very different.

However, it is clear that the correction factor f model (represented by the blue dotted line), in addition to significantly increasing the accuracy of the shock wave capture, also corrects the total value of the droplet population (correspond to the zeroth order moment). The table.7 shows the difference in the position of the condensation wave using

the different nucleation rate models implemented in the SU2 solver for case 424.

Table 7: Numerical results for zeroth order Moment.

Nucleation Rate Theory	Onset Condensation Position	MoM(0)'s Value
CNT	9.256 cm	$1.34 \; . \; 10^{19}$
ICCT	9.688 cm	$1.38 \; . \; 10^{19}$
Factor f	11.072 cm	$1.88 \; . \; 10^{18}$

4.4.3 TEST CASE D: Arina's nozzle 3D

The he author also simulated a three-dimensional model of condensation in metastable conditions for the modified geometry of Arina's nozzle, mentioned earlier in this work. This new geometry has a central body inside, being able to generate a swirl in the flow. All the calculations are performed on a 800,000 cells grid. The set of boundary conditions for the simulations are summarized in table.8.

Table 8: Flow parameters and boundaries conditions for a Test Case D.

Fluid	H_2O
Physical Problem	EULER
EoS	iPRSV
Gas Constant	461.51(J/Kg*K)
Specific heat ratio	1.29
Critical Temperature	647.12 K
Critical Pressure	$22060000 N/m^2$
Critical Density	322 Kg/m ^{3}
Inlet Total Pressure	39996,71 Pa
Inlet Total Temperature	376,15 K
Static outlet pressure	9999.175 Pa
Spatial scheme	ROE - $1°order$

The effects of the swirl generator can be seen through Fig.20, representing the pressure profile along the entire nozzle. The Fig.21, shows that code is able to successfully simulate the condensation phenomena in more complex three-dimensional geometries. The entire blue region represents the absence of droplet populations up to the point x = 0.65 cm. From that point, the droplet population finds the necessary conditions to increase

its value (green region).

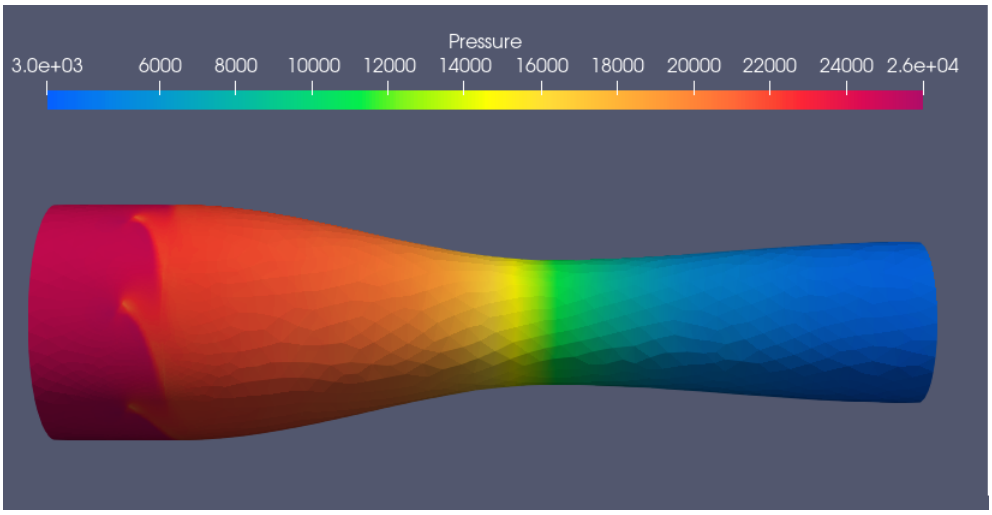

Figure 20: Pressure profile for a three-dimensional mesh: Arina 's nozzle with swirl generator.
Source: Author

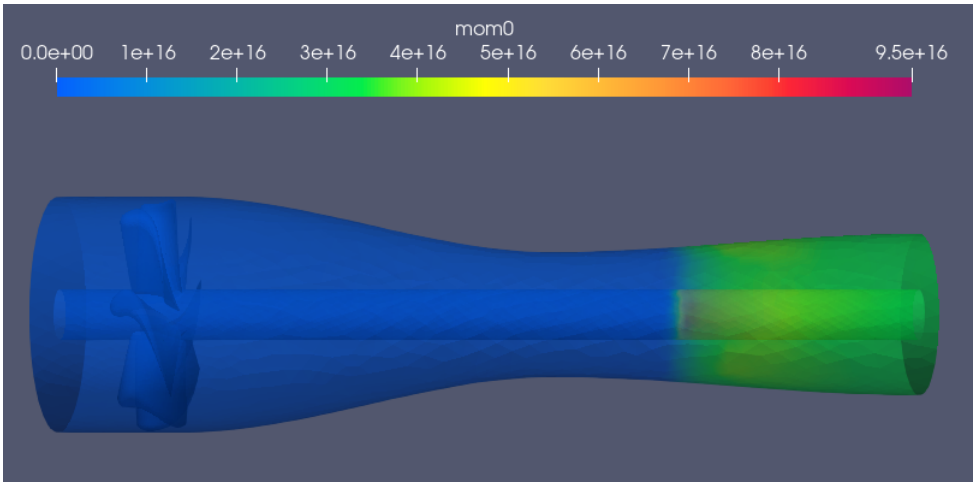

Figure 21: The zeroth order moment for a three-dimensional mesh: Arina 's nozzle with swirl generator.
Source: Author

For a better understanding of the condensation phenomenon, Fig.22 shows the Mach profile along the nozzle, downstream of the throat. The analysis starts at the point x = 0.6 cm, just before the droplet formation begins. As the first nuclei of the new liquid phase grow, the heat released in the surrounding gas mixture due to the phase transition increases the temperature and pressure, and consequently, the velocity of flow drops momentarily. It is possible to observe that the Mach number falls between the points x =

0.64cm to x = 0.7cm.

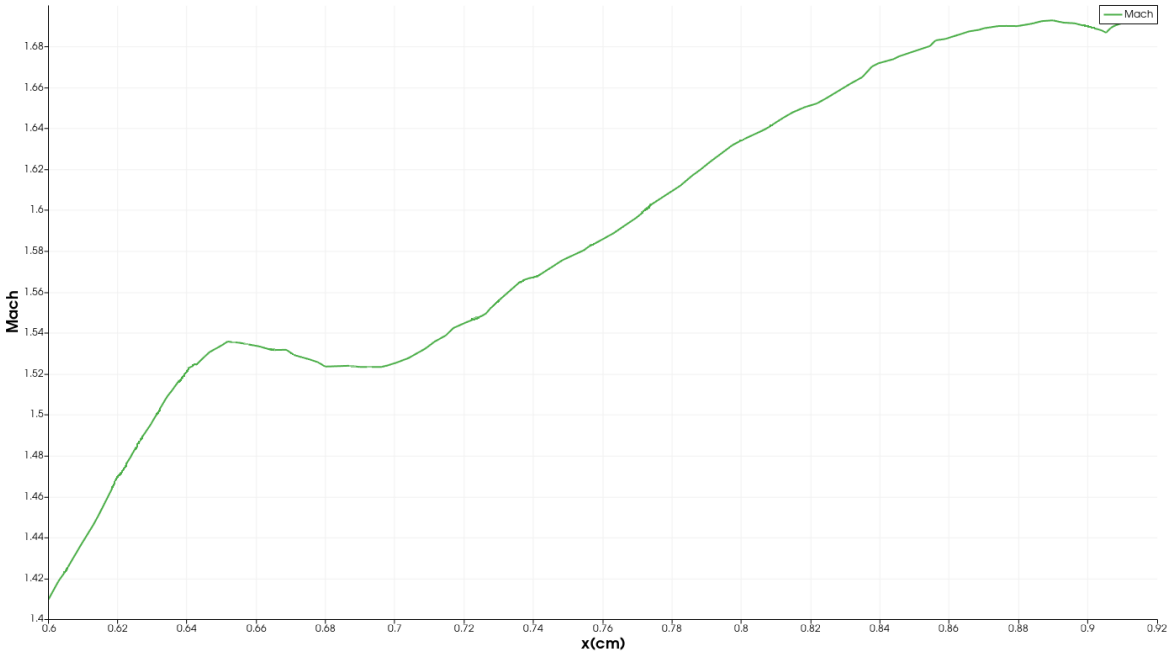

Figure 22: Mach profile fo a three-dimensional mesh: Arina's nozzle with swirl generator. Source: Author

The Figures 23, 24 and 25 represent the zeroth order moment (MoM 0), the first order moment(MoM 1) and second order moment(MoM 2),respectively. These results demonstrate the code's efficiency in reproducing Hill's Moments Method.

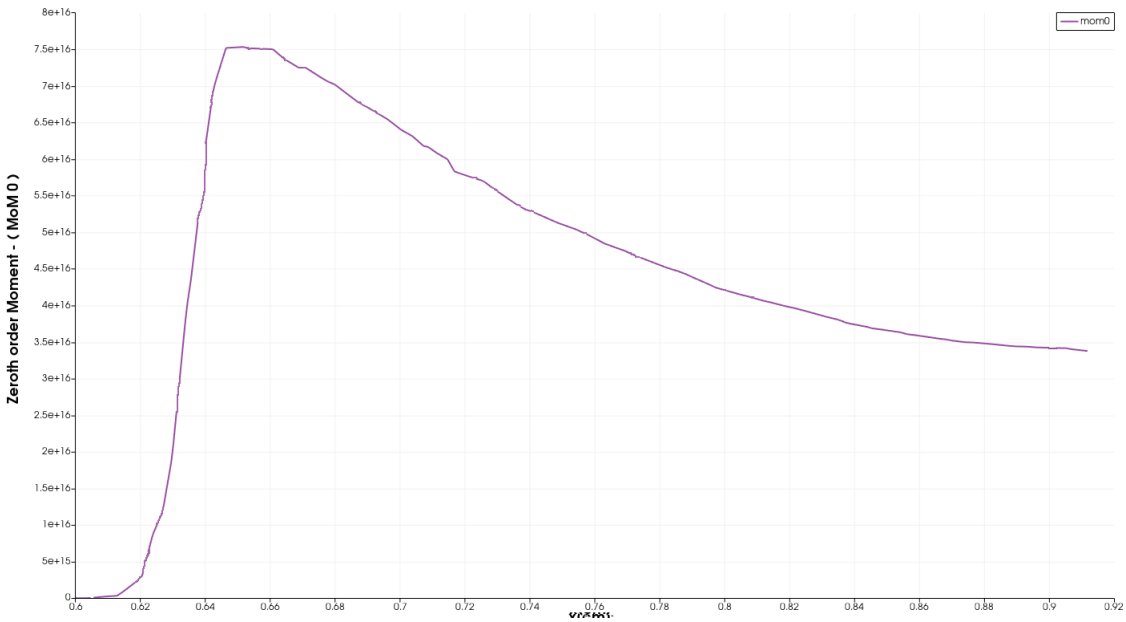

Figure 23: The zeroth order moment profile for a three-dimensional mesh: Arina's nozzle with swirl generator.
Source: Author

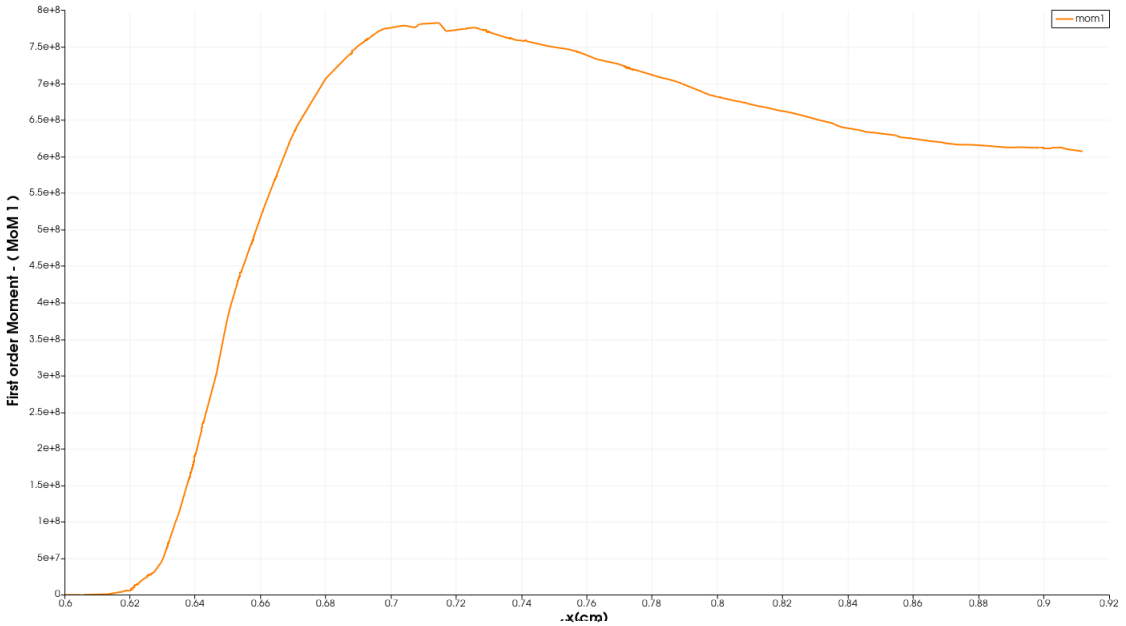

Figure 24: The first order moment profile for a three-dimensional mesh: Arina's nozzle with swirl generator.
Source: Author

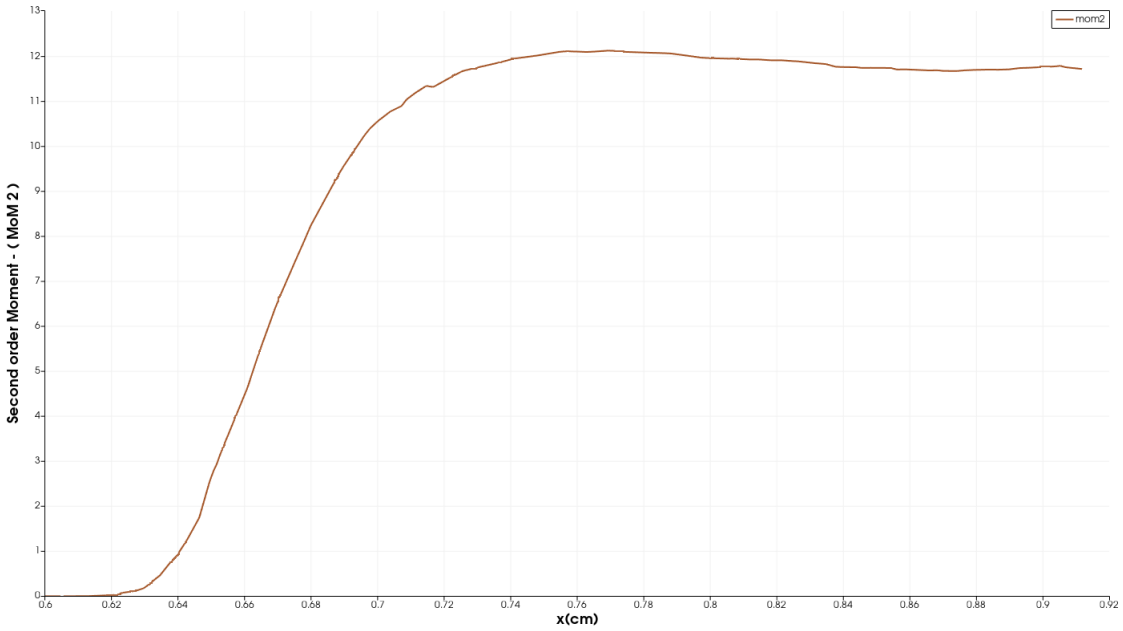

Figure 25: The second order moment for a three-dimensional mesh: Arina's nozzle with swirl generator.
Source: Author

Although a mesh of 800000 elements is considered insufficient to represent the physics of the problem of this complexity, the code was able to successfully capture the condensation phenomena. The condensation wave did not appear completely, however, this can be solved, increasing the refinement of the mesh.

5 CONCLUSIONS AND RECOMMENDATIONS

In this dissertation, the low-pressure condensing steam flows were investigated using the Method of Moments (MoM). The numerical results show that coupled nucleation models, such as the Hill's Method of Moments, can be used as a good approximation to analyze compressible flows in nozzle geometries.

Our numerical results indicated that the SU2 branch *feature-turbo2phase* is capable of successfully simulating the condensation phenomenon for two-dimensional and three-dimensional problems. The position of the condensation wave predicted by the numerical simulations is slightly different from the experimental results. This difference can be explained by the fact that our simulations did not take into account the viscous effects or the effects of turbulence. In addition, the only nucleation rate model implemented in the branch was the classic nucleation model (CNT). It is known that such a model has many limitations in relation to the capture of the condensation wave. Therefore, some discrepancies between numerical and experimental results were expected.

The challenge of numerically reproducing the exact point where the condensation wave occurs depends mainly on the precision of the nucleation rate equation used. The condensation models present in SU2 are still in a development version and as part of our contribution we have introduced two new models in the code: the Internally Consistent Classical Theory (ICCT) and the correction factor f suggested by the literature. The numerical results proved that the correction factor, besides being efficient to correct the position of the condensation wave, also corrects the total value of the droplet population (zeroth order moment) inside the supersonic separator.

Due to the deadlines for submitting this dissertation, only simulations involving water were performed. Although it is not the main objective of the supersonic separator device, the condensation of water vapor is quite relevant to our research. We can conclude that the numerical results are satisfactory for low-pressure condensation.

The following recommendation are drawn for future studies:

1. The correction factor proved to be efficient for low pressures. Additional data on high-pressure cases have to be included in the analysis in order to improve the modeling of supersonic flows processes, as they are more common to turbomachinery.

2. The classical nucleation theory (CNT) models provide to be not suitable in order to attain a higher level of accuracy in the simulation of condensing flows of organic fluids. Although the models implemented by the author (ICCT and the factor f) inside the SU2 code, are more accurate in the simulations presented in this dissertation, it is important to note that the numerical investigations were based on water vapor as a working fluid. Therefore, it is important to test such models with more complex molecules such as Carbon Dioxide (CO_2) and Methane(CH_4).

3. So far it is only possible to simulate condensation of a single component gas. Condensation for gas mixtures is not currently available on any SU2 branch and it is thus necessary to study thermodynamic models for gas mixtures in order to implement them on the SU2 code.

4. Investigate the effects of swirl on the condensation phenomena along the flow.

REFERENCES

PINI S. VITALE, P. C. G. G. A. G. T. J. F. M. (Ed.). *"SU2: the Open-Source Software for Non-ideal Compressible Flows"*, v. 1 de *821*, (821, v. 1). "1st International Seminar on Non-Ideal Compressible-Fluid Dynamics for Propulsion Power", [S.l.]: "Journal of Physic", 2017.

ABERYSTWYTH University. 2018. ⟨http://users.aber.ac.uk/ruw/teach/215/real.php⟩.

AITKEN, J. On boiling, condensing, freezing, and melting. *Transactions of the Royal Scottish Society of Arts*, IX, 1874.

ARINA, R. Numerical simulation of near-critical fluids. *Numerical Mathematics*, v. 51, 2004.

AZZINI, M. P. L. Numerical investigation of high pressure condensing flows in supersonic nozzles. *Journal of Physics: Conference Series*, 3 2017.

BINNIE, R. G. M. An electrical detector of condensation in high-velocity steam. *R.V Southwell*, 1941.

CHENG, S. Z. *Phase Transitions in Polymers*. [S.l.]: Copyright © 2008 Elsevier B.V., 2008. v. 1. (1, v. 1). ISBN 978-0-444-51911-5.

ENGO-ENGINEERING. 2017. ⟨http:www.engo3s.com⟩. Accessed: 2018-07-18.

EPE. *Custos de Gás Natural no Pré-Sal Brasileiro*. 2012. ⟨http://epe.gov.br/sites-pt/publicacoes-dados-abertos/publicacoes/PublicacoesArquivos/publicacao-368⟩.

FAKHARI, K. *Numerical Modeling and Investigation of Unsteady Phenomena in Condensing Flows of Industrial Steam Turbines*. Tese (Doutorado) — Delft University of Technology, 2017.

GIBBS, J. W. On the equilibrium of heterogeneous substances. *Transactions of the Connecticut Academy of Arts and Sciences*, III, 1875–1878.

GMESH. 2019. ⟨http://gmsh.info/⟩. Accessed: 2019-12-22.

GRUBEL J. STARZMANN, M. E. S. M.; VOGT, D. M. Modelling of condensing steam flows in laval nozzles with ansys cfx. *Proceedings of the Institution of Mechanical Engineers, Part A: Journal of Power and Energy*, v. 232, p. 571 – 575, 2018.

GYARMATHY, G. Nucleation of steam in high-pressure nozzle experiments. *Journal of Power and Energy*, 2015. ISSN 09576509.

HALAMA, J. Numerical simulation of steam condensation in a nozzle. *The European Physical Journal Conferences*, 4 2012.

J.I.YELLOT; HOLLAND, C. *The condensation of flowing steam: Condesantion in diverging nozzles*. [S.l.: s.n.], 1874. 703-705 p.

KEENAN, J. H. *Thermodynamics*. [S.l.]: Wiley, 1941.

KLEIN, M. The historical origins of the van der waals equation. *Physica*, v. 73, n. 1, p. 28 – 47, 1974. ISSN 0031-8914.

MONTEIRO J./ SILVA, J. *Gás Natural Aplicado à Industria e ao Grande Comércio*. [S.l.]: EDGAR BLUCHER, 2010. ISBN 8521205627.

MOSES, S. On the growth of steam droplets formed in a laval nozzle using both static pressure and light scattering measurements. *Trans. ASME J. Fluids*, v. 100, 1978.

NEDERSTIGT, P. *Real Gas Thermodynamics*. Dissertação (Mestrado) — Ruhr-University, 2010.

PENG, D.-Y.; ROBINSON, D. B. A new two-constant equation of state. *Fluid Phase Equilibria*, VI, p. 43–54, 1970.

STEVER, H. G. *Fundamentals of Gas Dynamics*. [S.l.]: Princeton Legacy, 1958.

STODOLA. *Steam and Gas Turbines*. [S.l.]: McGraw-Hill, 1927.

STRYJEK, R.; VERA, J. H. Prsv: An improved peng—robinson equation of state for pure compounds and mixtures. *The Canadian Journal of Chemical Engineering*, v. 64, n. 2, p. 323–333, 1986.

TWISTER. 2016. ⟨https://www.twisterbv.com/twister-supersonic/⟩. Accessed: 2018-07-18.

VITALE, S. et al. Extension of the SU2 open source CFD code to the simulation of turbulent flows of fluids modeled with complex thermo–physical laws. In: AIAA. *22nd AIAA Computational Fluid Dynamics Conference*. Dallas, TX, 2015. 2015–2760.

VOLMER, A. W. Z. M. Keimbildung in übersättigten gebilden. *Physikal. Chemie*, v. 199, p. 277–301, 1925. ISSN 0942-9352.

YOUNG, A. W. J. Homogeneous nucleation and shock wave interaction in condensing steam flows. *Acta Mechanica*, 1992.

APPENDIX A – ALPHA

A.1 Governing Equations in SU2

A.1.1 Compressible Navier-Stokes

The SU2 solves the compressible Navier-Stokes equations expressed in differential form as:

$$\Re(U) = \frac{\partial U}{\partial t} + \nabla.\bar{F}^c - \bar{F}^v(U, \nabla U) - S = 0 \tag{A.1}$$

where the conservative variables are the working variables and given by:

$$U = \{\rho, \rho\bar{v}E\}^T \tag{A.2}$$

the term S is a generic source term, and the convective and viscous fluxes are:

$$\bar{F}^c = \begin{Bmatrix} \rho\bar{v} \\ \rho\bar{v} \bigotimes \bar{v} + \bar{\bar{I}}p \\ \rho E\bar{v} + \rho\bar{v} \end{Bmatrix} \tag{A.3}$$

and

$$\bar{F}^v = \begin{Bmatrix} \cdot \\ \bar{\bar{\tau}} \\ \bar{\bar{\tau}}\bar{v} + \kappa\nabla T \end{Bmatrix} \tag{A.4}$$

where ρ is the fluid density, $\bar{v} = \{u, v, w\}^{\mathsf{T}} \in \mathbb{R}^3$ is the flow speed in Cartesian system of reference, E is the total energy per unit mass, p is the static pressure, τ is the viscous stress tensor, T is the temperature, κ is the thermal conductivity, and μ is the viscosity. The viscous stress tensor can be expressed in vector notation as:

$$\bar{\bar{\tau}} = \mu \left(\nabla \bar{v} + \nabla \bar{v}^T \right) - \mu \frac{2}{3} \bar{\bar{I}} \left(\nabla \cdot \bar{v} \right) \tag{A.5}$$

The thermal conductivity in the energy equation becomes an effective thermal conductivity written as:

$$\kappa = \frac{\mu_d \, c_p}{Pr_d} + \frac{\mu_t \, c_p}{Pr_t} \tag{A.6}$$

where we have introduced a turbulent Prandtl number Pr_t and μ_t is the turbulent viscosity .

A.1.2 Compressible Euler

Compressible Euler equations can be obtained by compressible Navier-Stokes equations by neglecting the terms for viscosity and thermal conductivity. That way we will have

$$\mathcal{R}(U) = \frac{\partial U}{\partial t} + \nabla \cdot \bar{F}^c(U) - S = 0 \tag{A.7}$$

where the conservative variables are the working variables and are given by

$$U = \{\rho, \rho\bar{v}, \rho E\}^{\mathsf{T}} \tag{A.8}$$

the term S is a generic source term, and the convective flux is

$$\bar{F}^c = \left\{ \begin{array}{c} \rho\bar{v} \\ \rho\bar{v} \otimes \bar{v} + \bar{\bar{I}}p \\ \rho E\bar{v} + p\bar{v} \end{array} \right\} \tag{A.9}$$

APPENDIX B – BETA

B.1 Arina's nozzle geometry

The geometry of nozzle used by Arina in his experiment is shown in Figure 26.

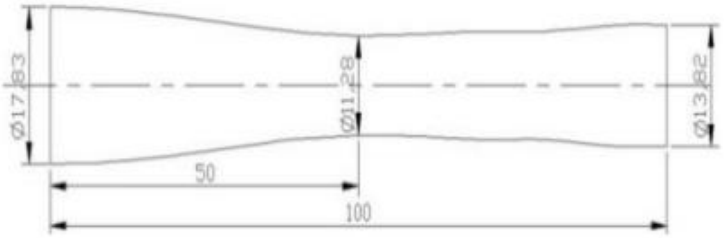

Figure 26: Arina's nozzle geometry
Source:[ARINA, 2004]

In order to simulate the test cases presented in this work, a multiblock unstructured 3D- mesh was generated with GMESH 4.0 . After an exhaustive study of mesh efficiency, we obtained two ideal meshes for this problem. The finer mesh will account up to approximately 860 thousand nodes, while a coarser mesh consists of around 150 thousand nodes (Figure 27).

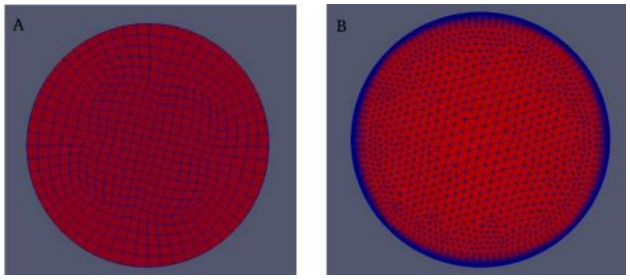

Figure 27: Front view of the 3D mesh. a) Coarse mesh with $1.8x10^5$ nodes. b) Fine mesh with $8.5x10^5$ nodes and wall refinement.
Source: Author

B.2 Moses and Stein's nozzle geometry

The geometry of nozzle used by Moses and Stein in his experiment is shown in Figure 28.

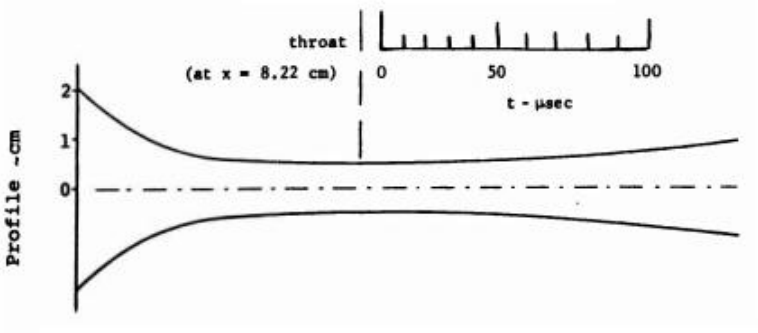

Figure 28: Moses and Stein's nozzle geometry
Source: [MOSES, 1978]

In order to simulate the test cases presented in this work, a multiblock unstructured 2D- mesh was generated with GMESH 4.0, with 50 000 nodes.

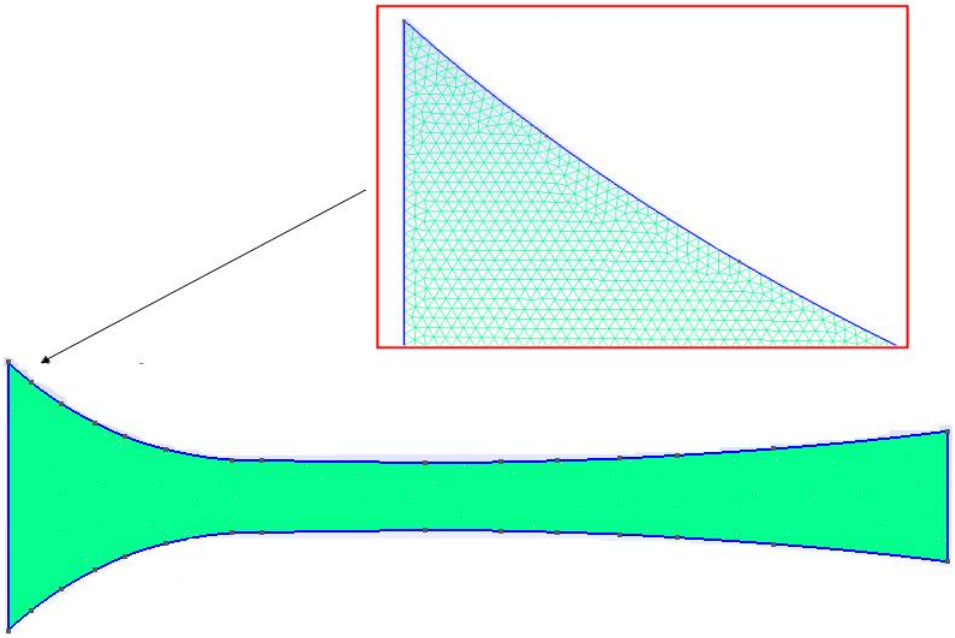

Figure 29: Moses and Stein's nozzle geometry
Source: Author

B.3 Binnie and Green 's nozzle geometry

The geometry of nozzle used by Binnie and Green in his experiment is shown in Figure 30.

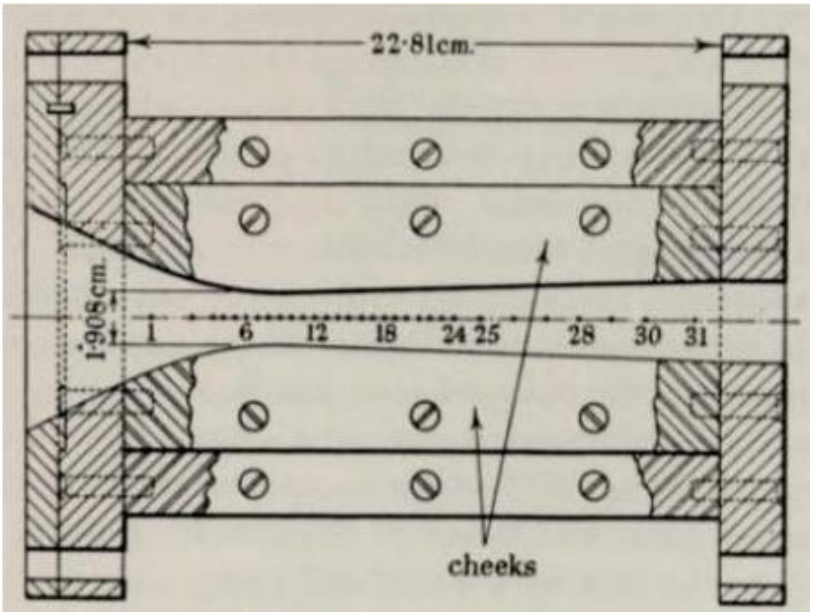

Figure 30: Nozzle profile reproduced from Binnie et al
Source: [BINNIE, 1941]